1 Factors controlling marine aerosol size distributions and
2 their climate effects over the Northwest Atlantic Ocean
3 region

5 Betty Croft[1], Randall V. Martin[2,1], Richard H. Moore[3], Luke D. Ziemba[3], Ewan C. Crosbie[3,4],

6 Hongyu Liu[5], Lynn M. Russell[6], Georges Saliba[6], Armin Wisthaler[7,8], Markus Müller[7],

7 Arne Schiller[7], Martí Galí[9], Rachel Y.-W. Chang[1], Erin E. McDuffie[1,2], Kelsey R. Bilsback[10],

8 and Jeffrey R. Pierce[10]

10 [1]Department of Physics and Atmospheric Science, Dalhousie University, Halifax, NS, Canada

11 [2]McKelvey School of Engineering, Washington University in St. Louis, St. Louis, MO, USA

12 [3]NASA Langley Research Center, Hampton, VA, USA

13 [4]Science Systems and Applications, Inc., Hampton, VA, USA

14 [5]National Institute of Aerospace, Hampton, VA, USA

15 [6]Scripps Institute of Oceanography, University of California, San Diego, La Jolla, CA, USA

16 [7]Institute for Ion Physics and Applied Physics, University of Innsbruck, Technikerstrasse 25,

17 6020 Innsbruck, Austria

18 [8]Department of Chemistry, University of Oslo, P.O. 1033 – Blindern, 0315 Oslo, Norway

19 [9]Barcelona Supercomputing Center (BSC)

20 [10]Department of Atmospheric Science, Colorado State University, Fort Collins, CO, USA

21 *Correspondence to:* Betty Croft (betty.croft@dal.ca)

23 **Abstract.**

24 Aerosols over Earth's remote and spatially extensive ocean surfaces have important influences on

25 planetary climate. However, these aerosols and their effects remain poorly understood, in part due

26 to the remoteness and limited observations over these regions. In this study, we seek to understand

27 factors that shape marine aerosol size distributions and composition in the Northwest Atlantic

28 Ocean region. We use the GEOS-Chem-TOMAS model to interpret measurements collected from

29 ship and aircraft during the four seasonal campaigns of the North Atlantic Aerosols and Marine

30 Ecosystems Study (NAAMES) conducted between 2015 and 2018. Observations from the

31 NAAMES campaigns show enhancements in aerosol total number concentration at atmospheric

32   altitudes of about 1 km, most pronounced during the phytoplankton bloom maxima (May/June).

33   Our simulations, combined with NAAMES ship and aircraft measurements, suggest several key

34   factors contribute to aerosol number and size in the Northwest Atlantic lower troposphere, with

35   significant regional-mean (40-60 °N, 20-50 °W) aerosol-cloud albedo indirect effects (AIE) and

36   direct radiative effects (DRE) during the phytoplankton bloom. These key factors and their

37   associated radiative effects in the region are: (1) particle formation above/near the marine

38   boundary layer (MBL) top (AIE: -3.37 W m^{-2}, DRE: -0.62 W m^{-2}), (2) particle growth due to

39   marine secondary organic aerosol (MSOA) as the nascent particles subside into the MBL, enabling

40   them to become cloud-condensation-nuclei-size particles (AIE: -2.27 W m^{-2}, DRE: -0.10 W m^{-2}),

41   (3) particle formation/growth due to the products of dimethyl sulfide, above/within the MBL (-

42   1.29 W m^{-2}, DRE: -0.06 W m^{-2}), and (4) ship emissions (AIE: -0.62 W m^{-2}, DRE: -0.05 W m^{-2}).

43   Our results suggest a synergy of particle formation near the MBL top and growth by MSOA that

44   contributes strongly to cloud-condensation-nuclei-sized particles with significant regional

45   radiative effects in the Northwest Atlantic. Future work is needed to understand the sources and

46   temperature-dependence of condensable marine vapors forming MSOA and to understand the

47   species that can form new particles at the boundary layer top and grow these particles as they

48   descend into the marine boundary layer.

50   1. Introduction

52   Marine atmospheric particles have important roles in Earth's climate system. Similar to particles

53   in other regions, marine aerosols scatter and absorb solar radiation (Charlson et al., 1992), and

54   modify cloud properties by acting as the seeds for cloud droplet formation (Boucher and Haywood,

55   2000; Lohmann and Feichter, 2005). Aerosols in the atmosphere's marine boundary layer (MBL)

56   strongly influence the highly prevalent, low-altitude marine clouds, which have key climate

57   cooling effects due to their reflection of incoming solar radiation (Wood, 2012; Chen et al., 2014).

58   However, there remains high uncertainty about the magnitude of these aerosol effects (IPCC,

59   2013), due in part to limited understanding about the processes that control aerosols over Earth's

60   expansive and remote ocean surfaces (Willis et al., 2018). Marine aerosols are strongly influenced

61   by natural, but poorly understood sources, making a large contribution to uncertainty in aerosol-

62   climate effects (Carslaw et al., 2010; Carslaw et al., 2013). Limited observations of aerosols and

63   their precursors over Earth's remote marine regions contribute to these knowledge gaps. In this

64   study, we focus on investigation of factors controlling the seasonal cycle of aerosol size and

65   number and the resultant climate effects over the Northwest Atlantic Ocean.

66

67   Aerosol particles in the remote MBL have several seasonally varying sources (O'Dowd et al.,

68   2004; Leck and Bigg, 2005; de Leeuw et al., 2011; Karl et al., 2012). Primary particles are emitted

69   through wave breaking and bubble bursting processes that eject sea spray aerosols (SSA) of sea

70   salt and organic composition (Russell et al., 2010; de Leeuw et al., 2011; Ovadnevaite et al., 2011;

71   Gantt and Meskhidze, 2013; Prather et al., 2013; Hamacher-Barth et al., 2016; Brooks and

72   Thornton, 2018). SSA have a dependence on wind speed (Monahan et al., 1983; O'Dowd et al.,

73   1997; Ovadnevaite et al., 2012; Grassian et al., 2015; Brooks and Thornton, 2018; Saliba et al.,

74   2019) and sea surface temperature (Mårtensson et al., 2003; Jaeglé et al., 2011; Kasparian et al.,

75   2017; Saliba et al., 2019). For the North Atlantic, observations indicate that primary SSA make a

76   limited (less than 30%) contribution to cloud condensation nuclei (CCN) (Quinn et al., 2017,

77   Zheng et al., 2018; Quinn et al., 2019) with no direct connection between SSA emissions and

78   plankton ecosystems because the organic SSA appears to arise from the ocean's large pool of

79   dissolved organic carbon (Quinn et al., 2014; Bates et al., 2020). SSA, however, could modify the

80   CCN number that activate to form cloud droplets (Fossum et al., 2020), act as ice nuclei (Wilson

81   et al., 2015; DeMott et al., 2016; Irish et al., 2017), and be more closely linked with biogenic

82   activity in other regions (Ault et al., 2013; Cravigan et al., 2015; O'Dowd et al., 2015; Quinn et

83   al., 2015; Wang et al., 2015; Schiffer et al., 2018; Cravigan et al., 2019). For the North Atlantic,

84   secondary aerosol of biogenic origin is observed to be an important seasonally varying contributor

85   to marine particles and their growth to yield CCN (Sanchez et al., 2018). Marine secondary aerosol

86   can arise from the condensation of a variety of marine-vapor-oxidation products, which form and

87   grow particles (Ceburnis et al., 2008; Rinaldi et al., 2010; Decesari et al., 2011). Formation of new

88   aerosol particles in the marine environment is observed to be favored in clean atmospheric layers

89   just below the marine inversion and also above the MBL top (Kazil et al., 2011; Takegawa et al.,

90   2020). Newly formed particles can grow to CCN sizes (diameters larger than about 50 nm) through

91   the condensation of available organic and sulfur-containing vapors while descending in the MBL

92   (Korhonen et al., 2008). Once the particles reach CCN sizes, cloud processing (including aqueous

93   phase aerosol production, and cloud droplet coagulation with other droplets and interstitial

94   aerosols) also contributes to shaping the size distribution (Hoppel et al., 1986; Hoose et al., 2008;

95   Pierce et al., 2015). For the North Atlantic MBL, entrainment of growing new particles formed in

96   the relatively cleaner free troposphere is an important contributor to MBL particle number (Quinn

97   et al., 2017; Sanchez et al., 2018; Zheng et al., 2018). In the pristine conditions of the summertime

98   Arctic, both new particle formation (NPF) and growth (by condensation of organic and sulfur-

99   containing vapors) are frequently observed within the boundary layer itself (Leaitch et al., 2013;

100 Croft et al., 2016a; Willis et al., 2016; Collins et al., 2017; Burkart et al., 2017b). In addition to

101 sulfuric acid, other vapors including amines, methane sulfonic acid (MSA), ammonia, and iodine

102 all contribute to NPF in marine regions (O'Dowd, 2002; Facchini et al., 2008; Allan et al., 2015,

103 Chen et al., 2016; Croft et al., 2016a; Dall´Osto et al., 2018). Interpretation of a combination of

104 aircraft and ship-board observations with a size-resolved aerosol microphysics model is needed to

105 develop understanding of the relative importance of above-/near-MBL-top NPF as a contributor

106 to aerosol size distributions in the Northwest Atlantic MBL.

107

108 Dimethyl sulfide (DMS) is one of the key contributors to secondary particle formation and growth

109 that is released from the oceans as a result of marine biogenic activity (Lana et al., 2012a; Galí and

110 Simó, 2015; Sanchez et al., 2018). The oxidation products of DMS include sulfuric acid and MSA

111 (Barnes et al., 2006), which can form new particles and grow existing particles to sizes that can

112 act as CCN (Hoffman et al., 2016; Hodshire et al., 2019). As well, hydroperoxymethyl thioformate

113 (HPMTF) is a recently discovered DMS-oxidation product, which could also contribute to NPF

114 and growth (Veres et al., 2020). The role of DMS in the climate system has undergone much debate

115 since 1987 when the CLAW hypothesis proposed that DMS could act as a regulator in a warming

116 climate (Charlson et al., 1987). For the North Atlantic and Arctic, observations have linked DMS

117 to the formation of aerosols during the times of phytoplankton blooms (Rempillo et al., 2011;

118 Chang et al., 2011; Park et al., 2017; Sanchez et al., 2018; Abbatt et al., 2019; Quinn et al., 2019).

119 As well, modelling studies have supported a role for DMS, linked to phytoplankton blooms, as a

120 contributor to CCN number concentrations in the North Atlantic and Arctic MBLs (Woodhouse et

121 al., 2013; Zheng et al., 2018; Ghahremaninezhad et al., 2019; Mahmood et al., 2019) and Southern

122 Ocean MBL (Korhonen et al., 2008; McCoy et al., 2015; Revell et al., 2019). However, the extent

123 to which DMS can act as a climate regulator remains unclear (Schwinger et al., 2017; Fiddes et

124 al., 2018), and this role has been refuted (Quinn and Bates, 2011). Analysis of in situ observations

125   of DMS and its products across the seasonal cycle of marine biogenic activity and in various ocean

126   regions is needed to improve understanding related to the role of DMS in Earth's climate system.

127

128   Marine secondary organic aerosol (SOA) is another important contributor to sub-micron diameter

129   marine aerosols, but is not well characterized (Rinaldi et al., 2010). The oceans are a source of a

130   variety of organic vapors that could lead to SOA formation (O'Dowd and de Leeuw, 2007; Yassaa

131   et al., 2008; Carpenter et al., 2012; Lana et al. 2012b; Hu et al., 2013; Carpenter and Nightingale,

132   2015; Kim et al., 2017; Rodríguez-Ros et al., 2020a). Oxygenated volatile organic compounds

133   (OVOCs) recently linked to photochemical oxidative processes at the sea surface microlayer are

134   possible contributors to marine SOA (Mungall et al., 2017). Isoprene and monoterpenes appear to

135   make relatively minor contributions to marine SOA by mass, less than 1% for particles with

136   diameters smaller than 10 μm at Cape Grim (Cui et al., 2019). The global, annual source of organic

137   vapors from the oceans is highly uncertain, but current estimates are about 23.2 to 91.9 Tg C yr^{-1}

138   (Brüggemann et al., 2018). Laboratory studies indicate that emissions of marine organic vapors

139   increase with both temperature and incident radiation for temperatures up to about 26 ℃

140   (Meskhidze et al., 2015). Recent observations and modeling studies support a role for Arctic

141   marine secondary organic aerosol (AMSOA) as a contributor to particle growth to CCN sizes

142   (Burkart et al., 2017a; Collins et al., 2017; Willis et al, 2017; Willis et al., 2018; Tremblay et al.,

143   2018; Leaitch et al., 2018; Croft et al., 2019; Abbatt et al., 2019). For the North Atlantic, organics

144   are also found to make a large contribution to particle growth to CCN sizes. (Sanchez et al., 2018;

145   Zheng et al., 2020a). The result of the above-noted processes is a large and complex pool of organic

146   aerosol in the marine environment with sources that vary seasonally and regionally (Cavalli et al.,

147   2004; Decesari et al., 2011; Cravigan et al., 2015; Liu et al., 2018; Leaitch et al., 2018).

148

149   Anthropogenic activity is also an important source of aerosols over the portions of the Earth's

150   oceans. For the North Atlantic, several previous studies (e.g. Savoie et al., 2002; Stohl et al., 2003;

151   Huntrieser et al., 2005; Fast et al., 2016) found a key role for synoptic scale motions in lifting

152   aerosols arising from North American continental emissions and transporting them in layers over

153   the North Atlantic with intrusions into the MBL. As well, ship traffic is an important source of

154   both particles and oxidants in the MBL (Corbett et al., 2007; Zanatta et al., 2019; Bilsback et al.,

155 submitted). Ship emissions of nitrogen oxides have a significant control on levels of oxidants such

156 as ozone, the hydroxyl radical (OH) and NO_3 in the MBL (Vinken et al., 2011; Holmes et al.,

157 2014). In the remote MBL, both OH and NO_3 are key oxidants of DMS, along with natural-source

158 halogens such as BrO, with an important role for multiphase chemistry (Chen et al., 2018).

159 Interpretation of aerosol observations across several seasons is needed to better understand the

160 relative contribution of ship emissions to marine particles in the Northwest Atlantic region.

161

162 In this study, as part of the Ocean Frontier Institute (www.oceanfrontierinstitute.com), we address

163 the knowledge gaps that were identified above, concerning several key factors shaping Northwest

164 Atlantic MBL aerosol size distributions and their seasonal cycle. We consider the role of (1) new

165 particle formation in clean atmospheric layers near/above the MBL top, (2) particle growth by

166 marine SOA (MSOA) on descent into the MBL, (3) DMS contributions and (4) ship traffic

167 emissions. Aerosol measurements from the North Atlantic Aerosols and Marine Ecosystems Study

168 (NAAMES) (Behrenfeld et al., 2019) provide an excellent basis for addressing the role of these

169 four factors in the Northwest Atlantic Ocean region. The NAAMES aircraft and ship campaigns

170 were conducted during four phases of the Northwest Atlantic annual plankton cycle from 2015-

171 2018. We interpret the NAAMES aerosol measurements using a state-of-the-science size-resolved

172 global aerosol microphysics model, GEOS-Chem-TOMAS (www.geos-chem.org). Our

173 synergistic approach in bringing together NAAMES measurements and size-resolved aerosol

174 process modeling enables a unique consideration of factors shaping Northwest Atlantic MBL

175 aerosol size distributions and their annual cycle. We also quantify the impact of these factors on

176 aerosol radiative effects over the North Atlantic.

177

178 The second section provides an overview of our measurement and modeling methodology. The

179 third section presents results using the GEOS-Chem-TOMAS model to interpret NAAMES

180 aerosol measurements and their seasonal cycle with a focus on the roles of above/near-MBL-top

181 NPF, MSOA, DMS and ship emissions. We also quantify the direct and cloud-albedo indirect

182 aerosol radiative effects attributed to each of these factors during the seasonal cycle. The final

183 section gives our summary and outlook.

184

185 **2. Methodology**

186

2.1 Aerosol measurements during the NAAMES campaigns

NAAMES campaigns were conducted during four key periods in the annual cycle of marine biogenic activity, namely: the winter transition (November 2015), the accumulating phase (March/April 2018), the climax transition (May/June 2016), and the declining phase (August/September 2017) (Behrenfeld et al., 2019). These periods are defined by shifts in net phytoplankton growth rates and span a wide range in phytoplankton biomass, here estimated from chlorophyll-*a* concentrations (Chl-*a*). The winter transition is characterized by the annual minimum in Chl-*a* concentrations (generally < 1 mg m^{-3}) and a shift to favor phytoplankton growth over loss as the increasing ocean mixed-layer depth leads to fewer encounters between phytoplankton and their grazers. The accumulation phase occurs in early springtime when increasing sunlight and decreasing ocean mixed layer depths promote increasing phytoplankton growth rates and concentrations (Chl-*a* between 1 and 2 mg m^{-3}). The climax transition is the time of the annual maximum in phytoplankton biomass (Chl-*a* between 2 and 9 mg m^{-3}) and marks the shift from positive to negative growth rates owing to high grazing rates and depletion of nutrients. The declining phase (Chl-*a* between 1 and 2 mg m^{-3}) occurs later in the summertime when the ocean mixed layer depth increases and incident sunlight decreases, leading to further declines in phytoplankton growth and concentrations. Behrenfeld et al. (2019) provide an overview of the four measurement campaigns, and further details about Chl-*a* during NAAMES. The R/V Atlantis cruise tracks and NASA C130 flight paths are shown in Figure 1. Due to aircraft mechanical problems, there were no flights in 2018 during the accumulating phase.

In this study, we examine the NAAMES size-resolved aerosol measurements (particle diameters 20 to 500 nm) from the Scanning Electrical Mobility Sizer (SEMS, Model 138, 2002, BMI, Hayward, CA) aboard the R/V Atlantis ship. Aerosol particles were isokinetically drawn through an inlet positioned 18 m above sea level (Bates et al. 2002) and were subsequently dried below 20% relative humidity using silica diffusion driers prior to sampling by the SEMS. Clean marine periods were identified with criteria of relative wind directions within 90º of the bow, condensation nuclei number concentrations less than 2000 cm^{-3}, ammonium and organic aerosol not covarying, ammonium < 100 ng m^{-3} and having back trajectories primarily over the ocean surface. We also consider aerosol size-resolved measurements (particle diameters 10 to 282 nm) from the Scanning

218   Mobility Particle Sizer (SMPS, TSI Inc., Shoreview, MN) aboard the C130 aircraft. As well, we

219   give attention to measurements of total particle number concentration from the Condensation

220   Particle Counters (CPCs) with differing nominal lower detection diameters: 3 nm for the CPC

221   3025 and 10 nm for the CPC 3772 (TSI Inc., St. Paul, MN) aboard the C130 aircraft. We also

222   consider submicron, non-refractory sulfate (SO_4^-) and organic mass (OM) concentrations from an

223   Aerodyne High Resolution Time-of-Flight Aerosol Mass Spectrometer (HR-ToF-AMS, DeCarlo

224   et al., 2006) and refractory black carbon from the Single Particle Soot Photometer (SP2, Schwarz

225   et al., 2006) aboard the aircraft. HR-ToF-AMS and SP2 measurements are restricted to

226   accumulation-mode aerosol (60-600 nm and 105-600 nm diameter, respectively). All aircraft

227   observations are made behind a forward-facing, shrouded, solid diffuser inlet that efficiently

228   transmits particles with aerodynamic diameter less than 5.0 µm to cabin-mounted instrumentation

229   (McNaughton et al., 2007). Cloud-contaminated aerosol observations have been removed using a

230   combination of wing-mounted cloud probe and relative humidity measurements. This filtering may

231   possibly obscure some NPF events in proximity to clouds and remove some cloud-processed

232   samples from the vertical profiles. Aerosol number and mass concentrations are reported at

233   standard temperature and pressure. A Proton-Transfer-Reaction Time-of-Flight Mass

234   Spectrometer (PTR-ToF-MS) (Müller et al, 2014; Schiller, 2018) was used aboard the NASA C-

235   130 to measure volatile organic compounds including DMS and acetonitrile. Both observational

236   and model data for periods where acetonitrile concentrations exceed 200 ppt are filtered out

237   following Singh et al. (2012) to remove significant biomass burning contributions that are not the

238   focus of this study.

239

240   **2.2 GEOS-Chem-TOMAS model description**

241

242   We use the GEOS-Chem model (v12.1.1) (http://www.geos-chem.org) coupled to the TwO

243   Moment Aerosol Sectional (TOMAS) microphysics scheme (Adams and Seinfeld, 2002; Lee and

244   Adams, 2012; Kodros and Pierce, 2017), with 15 sections, representing particle sizes from 3 nm

245   to 10 µm. All simulations in this study are at a 4º × 5º resolution with 47 vertical levels extending

246   to 0.01 hPa. The meteorological fields are from the GEOS Forward Processing off-line fields

247   (GEOS-FP; https://gmao.gsfc.nasa.gov/GMAO_products/). Our size-resolved aerosol simulations

248   parameterize the processes of particle nucleation, coagulation, condensation, along with wet and

249   dry deposition and include the in-cloud aerosol coagulation scheme of Pierce et al. (2015). Sulfate,

250   organic and black carbon, sea salt, dust and aerosol water are simulated. TOMAS is coupled to the

251   full tropospheric aerosol/chemistry scheme of GEOS-Chem. Wet deposition follows Liu et al.

252   (2001), Wang et al. (2011) and Wang et al. (2014). To represent efficient wet removal by North

253   Atlantic drizzle in October and November, we implement a fixed in-cloud removal efficiency of

254   0.001 s^{-1} in the lowest 2 km of the model atmosphere over the ice-free ocean and enable wet

255   removal of sulfate and organic aerosol in clouds with temperatures between 237 K and 258 K. In

256   all seasons, we use the GEOS-FP cloud fraction as the precipitation fraction in the model layers

257   where precipitation occurs for a closer connection with the meteorological fields (Croft et al.,

258   2016b; Luo et al., 2019; Luo et al., 2020). Dry deposition uses the resistance in series approach of

259   Wesley (1989). Simulated gas-phase species are also removed by dry and wet deposition as

260   described in Amos et al. (2012).

261   Particle nucleation is parameterized with the ternary (H_2SO_4-NH_3-H_2O) scheme of Napari et al.

262   (2002), which was scaled by 10^{-5} to better match boundary-layer measurements (Westervelt, 2013)

263   and the binary (H_2SO_4-H_2O) scheme of Vehkamaki et al. (2002) at low NH_3 concentrations.

264   Growth and loss of particles smaller than 3 nm are approximated following Kerminen et al. (2004).

265   As a surrogate for unparameterized processes near the MBL top, we also employ an activation-

266   type nucleation parameterization from the MBL top to about 2 km altitude. This activation-type

267   scheme parameterizes nucleation rates as a linear function of sulfuric acid concentrations, using

268   an empirical factor ($A = 2 \times 10^{-6}$ s^{-1}) (Kulmala et al., 2006; Sihto et al., 2006), and serves as a

269   proxy representing the following unknown/unparameterized mechanisms related to NPF. Pockets

270   of very clean air with low condensation sink near MBL clouds, which favor new particle formation

271   (Kazil et al., 2011), are not resolved by large-scale models such as ours, with grid boxes on the

272   scale of 100s km^2. Efficient wet removal by drizzling MBL clouds contributes to these pristine

273   conditions (Wood et al., 2017). As well, MBL clouds reflect ultraviolet (UV) radiation and create

274   pockets of enhanced UV, which favors photochemical production of aerosol precursor vapors

275   (Weber et al., 2001; Wehner et al., 2015), and are not resolved by our model. Additionally, the

276   particle nucleating capacity of MSOA is unclear and particle formation parameterizations are not

277   yet developed to represent NPF when several gas-phase precursors interact. These precursors

278   include, but are not limited to, MSA (Chen et al., 2016), HPMTF (Veres et al., 2020), amines

279   (Facchini et al., 2008), iodine (Allan et al., 2015), and other extremely low-volatility organic

280   compounds (ELVOCs) (Riccobono et al., 2014).

281

282   For emissions, we use the GEOS-Chem v 12.1.1 default setup for gas-phase and primary aerosol

283   emissions. We use emissions from the Community Emissions Data System (CEDS) for global

284   anthropogenic sources of NO_x, CO, SO_2, NH_3, non-methane VOCs, black carbon, and organic

285   carbon, including from international shipping as a source of both primary and secondary particles.

286   Primary particles are emitted with a lognormal distribution (Lee et al., 2013). The most recent

287   CEDS emissions dataset extends to the year 2017, as described in McDuffie et al. (2020). In this

288   work, monthly CEDS emission totals for each compound are spatially gridded by source sector,

289   according to the $0.1° \times 0.1°$ gridded EDGAR v4.2 emissions inventory (EC-JRC/PBL, 2012) and

290   population, as described in Hoesly et al. (2018). To account for in-plume chemical processing of

291   ship emissions, we use the PARANOX scheme of Holmes et al. (2014). CEDS emissions are

292   overwritten over the United States by the National Emissions Inventory (NEI11) with updated

293   scale factors for our simulation years (2015-2018). We calculated these factors based on emission

294   data for these years from the United States Environmental Protection Agency. Over Canada, we

295   use the Air Pollutant Emissions Inventory (APEI). The Global Fire Emissions Database (GFED4s)

296   is used for biomass burning emissions (van der Werf et al., 2017) for the years 2015-2016, with

297   GFED4s climatological values for 2017 and 2018 since exact-year emissions were not available

298   when we conducted our simulations. Sea salt emissions follow Jaeglé et al. (2011). A coupled

299   parameterization for primary organic aerosol from sea spray was not available for our aerosol size-

300   resolved GEOS-Chem-TOMAS simulations, such that some organics could be misrepresented as

301   sea salt. Such primary organic emissions are expected to have no seasonal cycle when averaged

302   over the NAAMES region (Bates et al., 2020). Dust emissions are from the scheme of Zender et

303   al. (2003).

304

305   Exchange of DMS between the ocean and atmosphere is parameterized using the default GEOS-

306   Chem parameterization, which follows Johnson (2010), largely based on Nightingale et al. (2000a;

307   2000b). We use the 8-day mean satellite-retrieval seawater DMS dataset of Galí et al. (2019)

308   developed using the methodology of Galí et al. (2018), for available years (2015 and 2016) for the

309 region north of about 40 °N. The Lana et al. (2011) DMS climatology is used elsewhere. Terrestrial

310 biogenic emissions are from MEGAN2.1 as described in Guenther et al. (2012). Following Croft

311 et al. (2019), we add a source of MSOA coupled to the simple SOA scheme described in Pai et al.

312 (2020). Emissions of MSOA-precursor vapors have been found to increase with temperature

313 (Meskhidze et al., 2015; Rodríguez-Ros et al., 2020a; Rodríguez-Ros et al., 2020b). Here, we use

314 a temperature-dependent simulated source of MSOA-precursor emissions (S_{MSOA}), $S_{MSOA} = 70T$

315 $+ 350$ kg m^{-2} d^{-1}, where T is atmospheric temperature (°C) at 2 m altitude. The values of 70 and

316 350 are found to yield acceptable model-measurement agreement for the campaign-median ship-

317 track aerosol size distributions (Supplementary Fig. S1 and Table S1). The selected

318 parameterization also yielded agreement generally within the 25th to 75th percentiles of

319 measurements in the lowest 1 km of the atmosphere for the campaign-median vertical profiles of

320 total aerosol number (diameters larger than 3 nm, 10 nm, and between 3 and 10 nm) and integrated

321 SMPS number, as well as in the near-surface OM concentrations (Figs. S2-S4). This simulated

322 source of condensable vapors is emitted with a 50/50 split between vapors that are immediately

323 available to form MSOA and vapors with 1-day aging prior to availability (and not susceptible to

324 wet removal). MSOA contributes to particle growth in our simulations (in agreement with

325 observational-based studies e.g. Sanchez et al., 2018; Zheng et al., 2020a), along with sulfuric

326 acid, but since the particle nucleating abilities of MSOA are unclear, it does not contribute to new-

327 particle formation.

328

329 We also conduct off-line radiative transfer calculations using the Rapid Radiative Transfer Model

330 for Global Climate Models (RRTMG) (Iacono et al., 2008) to assess the direct radiative effect

331 (DRE) and cloud-albedo aerosol indirect effect (AIE). The aerosol optical properties are calculated

332 using the Mie code of Bohren and Hoffman (1983) to find the extinction efficiency, single

333 scattering albedo, and asymmetry factor. Then, these optical properties, along with the monthly

334 mean cloud fraction and surface albedo from the GEOS-FP meteorology fields, are input to the

335 RRTMG to determine the change in top-of-the-atmosphere solar flux (DRE) between two

336 simulations (our control simulation and one of the sensitivity simulations, Sect. 2.3). Our DRE

337 calculations follow Kodros et al. (2016), with updates to include ammonium nitrate as described

338 in Bilsback et al. (submitted). All particles except black carbon are treated as internally mixed

339 within each size section. We also calculate the cloud-albedo aerosol indirect effect (AIE) as

340   described in Kodros et al. (2016), Croft et al. (2016a) and Ramnarine et al. (2019). The Abdul-

341   Razzak and Ghan (2002) parameterization is used to calculate offline cloud droplet number

342   concentrations (CDNC) using the aerosol mass and number concentrations from our simulations.

343   We assume an updraft velocity of 0.5 m s^{-1} and the hygroscopicity parameters used by Kodros et

344   al. (2016) and Kodros and Pierce (2017), assuming aerosol internal mixture, including ammonium

345   nitrate following Bilsback et al. (submitted). For each model grid box, we assume cloud droplet

346   radii of 10 μm and perturb this value with the ratio of the monthly mean CDNC between two

347   simulations (our control simulation and one of the sensitivity simulations, Sect. 2.3), assuming

348   constant cloud liquid water content. The RRTMG is used to calculate the change in the top-of-the-

349   atmosphere solar flux (AIE) due to changes in cloud droplet radii.

350

351   As one evaluation of simulation performance, we calculate the mean fractional error (MFE) of the

352   0th to 3rd moments between the simulated and observed MBL aerosol size distributions, following

353   Boylan and Russell (2006) and using the same methodology as Hodshire et al. (2019) and Croft et

354   al., (2019). The MFE is defined as a mean over the N aerosol size distribution moments,

355

356   $$\text{MFE} = \frac{1}{N} \sum_{i=0}^{i=N-1} \frac{abs|C_m(i) - C_o(i)|}{(C_m(i) + C_o(i))/2} \qquad (1)$$

357

358   where $C_m(i)$ is the integrated value of the ith moment of the simulated aerosol size distribution and

359   $C_o(i)$ is the integrated value of the ith moment of the observed aerosol size distribution. The MFE

360   can range from 0 to +2. A MFE less than 0.5 is considered acceptable (Boylan and Russell, 2006).

361

362   **2.3 Summary of GEOS-Chem-TOMAS simulations**

363

364   Table 1 summarizes the simulations conducted. Simulation BASE is our control simulation and

365   includes all emissions and process parameterizations described above. We conduct four sensitivity

366   simulations to examine the role of several key factors involved in shaping the aerosol distributions

367   within the NAAMES study region. Simulation noABLNUC is the same as BASE, except without

368   the sulfuric acid-dependent activation-type surrogate nucleation parameterization, which we

369   implemented from the MBL top to about 2 km. Simulation noMSOA is the same as BASE, but

370   without the source of temperature-dependent condensable marine organic vapors, forming MSOA.

371 Simulation noDMS is the same as BASE, but without DMS. Finally, simulation noSHIPS is the
372 same as BASE, but without any ship emissions. All simulations are sampled using hourly output
373 along the NAAMES aircraft and ship tracks, using the NAAMES campaigns' 1-minute-resolution
374 navigation data.

375

376 **3. Results and Discussion**

377

378 **3.1 Key features of aerosols observed during NAAMES**

379

380 Aerosol observations made during the NAAMES campaigns were in four seasons, capturing
381 different stages of the annual cycle of Northwest Atlantic marine biogenic activity (Behrenfeld et
382 al., 2019). Figure 2 shows the campaign-median marine-influenced aerosol size distributions from
383 SEMS for the four R/V Atlantis cruises. November 2015 (winter transition, bloom minima) is
384 characterized by the lowest aerosol number concentrations. The peak of the Northwest Atlantic
385 drizzle season occurs at this time, with efficient wet removal of accumulation-sized aerosol
386 (diameters larger than about 50 to 100 nm) (Browse et al., 2012). As well, relative to other the
387 seasons, marine biogenic emissions are low at this time of minimal phytoplankton biomass. The
388 summertime observations during both May/June 2016 (climax transition, phytoplankton bloom
389 maxima) and August/September 2017 (declining phase) are characterized by a weakly dominant
390 Aitken mode (particle diameters < 100 nm). The winter transition (November 2015) and early
391 spring accumulation phase observations (March/April 2018) are characterized by the dominance
392 of accumulation-mode aerosols (particle diameters > 100 nm).

393

394 The vertical profiles of campaign-median integrated-SMPS (particle diameters of 10 to 282 nm)
395 observations are shown in Fig. 3. There are several key features of the observed aerosol vertical
396 profiles for the three NAAMES flight campaigns. These profiles exhibit particle number maxima
397 at about 1 km altitude during the May/June climax transition period. However, as shown in Fig. 3,
398 the aerosol surface and volume have a relative minimum at about 1-2 km. Lower particle surface
399 area favors new-particle formation over growth of pre-existing particles as available vapors
400 condense in these relatively cleaner atmospheric layers (Kazil et al., 2011). Transport of aerosols
401 (in part associated with continental emissions) is evident in all seasons at about 4-5 km altitude.

402   This is similar to the altitude of North Atlantic transport layers found by Fast et al. (2016). The

403   late fall (November 2015) is characterized by the lowest aerosol number, surface and volume

404   concentrations, similar to the findings shown in Fig. 2.

405

406   Figure 4 shows the vertical-profile campaign-median total particle number concentrations from

407   CPC, for aerosols with diameters larger than 3 nm (N3), larger than 10 nm (N10), and the

408   difference between the two (N3-N10). For the May/June 2016 climax transition (phytoplankton

409   bloom maximum), there is a strong enhancement in observed number concentration and variability

410   of sub-10 nm particles (N3-N10) between about 1 and 2 km altitude, indicating NPF at these

411   altitudes (Fig, 4, right column). This feature is near the MBL top, which ranged from about 0.5 to

412   2 km for the NAAMES cruises (Behrenfeld et al., 2019). Previous studies based on observations

413   from other marine regions have also found a cloud-processed ultra-clean layer with weak

414   condensation/coagulation sinks at about 1 km altitude, where NPF is favored (Kazil et al., 2011;

415   Takegawa et al., 2020). Figure 4 also shows enhancements in the observed N3 and N10

416   concentrations near and below 2 km during the summer months (climax transition and declining

417   phase). There is a relatively weaker N3, N10 and N3-N10 enhancement at about 2-3 km during

418   the winter transition (bloom minima). These low-altitude total number concentration

419   enhancements are most pronounced for during the phytoplankton bloom maximum, illustrating the

420   close connection between particle number and the level of marine biogenic activity.

421

422    $SO_4^=$ and OM are dominant non-refractory components of the submicron-diameter aerosols, and

423   vertical profiles of campaign-median observations are shown on Fig. 5. During the summertime

424   (May/June 2016, climax transition and August/September 2017, declining phase), the OM

425   contribution exceeds that of $SO_4^=$ at all altitudes up to 6 km. Non-refractory $SO_4^=$ has its peak

426   contribution during the climax transition season. This May/June phytoplankton bloom maxima

427   period is the time of peak observed near-surface atmospheric DMS mixing ratios, as shown in Fig.

428   6. During the climax transition (bloom maxima), non-refractory $SO_4^=$ concentrations increase

429   towards the surface, suggesting a marine surface source, similar to summertime Arctic marine

430   profile observations (Willis et al., 2017). Black carbon (BC) concentrations are also shown in Fig.

431   5 and are highest in the free troposphere for each NAAMES season, consistent with a long-range

432   transport source. BC concentrations peak in May/June, likely associated with greater transport of

433 anthropogenic continental pollution and biomass burning during this time, relative to other

434 seasons. Springtime has also been associated with peak BC concentrations in the Arctic due to

435 long-range transport (Sharma et al., 2004; Sharma et al., 2006; Fisher et al., 2010; Wang et al.,

436 2011; Xu et al., 2017). All aerosol mass concentrations in the lowest 2 km of the atmosphere (Fig.

437 5) are lowest in the November 2015 winter transition, which is a time of efficient wet removal by

438 drizzle (Browse et al., 2012; Wood et al., 2017), diminishing marine emissions due to diminishing

439 phytoplankton biomass, and outbreaks of relatively less polluted polar air advected down the

440 Labrador Strait (Behrenfeld et al., 2019). For the Arctic, the fall season has also been associated

441 with a relative minimum in aerosol number concentrations (Tunved et al., 2013; Croft et al.,

442 2016b).

443

444 The GEOS-Chem-TOMAS model (described in Sect. 2.2 and 2.3) is generally able to simulate the

445 above-noted features of the aerosols over the Northwest Atlantic. Simulation BASE captures key

446 aspects of the MBL size distributions including the minimum in aerosol number during the

447 November winter transition, the weakly dominant Aitken mode during the May/June climax

448 transition and August/September declining phase and the maximum in number of accumulation-

449 mode particles (diameters greater than 100 nm) during the March/April accumulation phase (Fig.

450 2). As well, the BASE simulation captures the lower tropospheric enhancements in particle number

451 concentration, although the simulated altitude for the maximum is sometimes displaced by a few

452 100 m (Figs. 3 and 4). In the lowest 2 km of the atmosphere, $SO_4^=$, OM, and BC mass

453 concentrations for simulation BASE are generally within the 25th to 75th measurement percentiles,

454 except for BC and OM underpredictions in May/June 2016, and OM overprediction in November

455 2015. All simulated $SO_4^=$ presented in this study is non-sea-salt $SO_4^=$. Simulation BASE also

456 captures that the near-surface $SO_4^=$ is greatest during the May/June climax transition and the near-

457 surface OM has its maximum value during the August/September declining phase. In the next four

458 sub-sections, we use the GEOS-Chem-TOMAS BASE simulation, relative to a set of sensitivity

459 simulations, to examine the potential of four key factors to shape aerosol size distributions in the

460 Northwest Atlantic during four stages of the annual cycle of marine biogenic activity.

461

462 **3.2 Role of new particle formation (NPF) near the MBL top**

463

464   Our simulations (BASE relative to noABLNUC, Fig. 4) suggest that NPF near/above the MBL has

465   a strong control on the development of the total particle number maxima near 1 km altitude, with

466   peak magnitude during the phytoplankton bloom maxima. This is particularly evident when

467   considering the N3-N10 concentrations in May/June (right column, Fig. 4). Figure 3 shows that

468   this NPF makes a significant contribution to simulated particle number concentrations for aerosol

469   diameters of 10 to 282 nm in the lowest 2 km of the atmosphere, most strongly in May/June (BASE

470   relative to noABLNUC). There is very little impact on aerosol mass concentrations for simulation

471   noABLNUC relative to BASE (Fig. 5).

472

473   NPF near/above the MBL top also makes a very strong indirect contribution to the simulated

474   aerosol size distributions within the MBL near the ocean surface (BASE versus noABLNUC, Fig.

475   2). In our simulations, NPF occurs near and above the MBL top, then the resultant particles grow

476   by condensation of available vapors and cloud processing while descending into the MBL. As a

477   result, the MBL-top NPF process contributes indirectly to near-ocean-surface particles, with

478   diameters from 20 to 200 nm. Table 2 shows that for all seasons, the MFE is acceptable (< 0.5,

479   following Boylan and Russell, (2006) with the surrogate nucleation (simulation BASE), and BASE

480   represents an improvement over simulation noABLNUC (without this surrogate NPF

481   parameterization).

482

483   **3.3 Role of particle growth by condensing marine organic vapors**

484

485   Condensing marine organic vapors forming MSOA are needed in our simulations (in addition to

486   H_2SO_4) for sufficient particle growth to yield satisfactory model-measurement agreement for MBL

487   size distributions (BASE versus noMSOA, Fig. 2). For simulation noMSOA, the model

488   overpredicts the number of particles with diameters smaller than about 30 nm in the MBL. Due to

489   insufficient particle growth of these sub-30 nm particles, the number of particles with diameters

490   between about 30 to 200 nm is underpredicted by more than 50% for simulation noMSOA.

491

492   In our simulations, MSOA enables particle growth to CCN sizes (diameters of about 50 nm or

493   larger). After particles reach CCN sizes, cloud processing can also contribute to simulated particle

494   growth towards accumulation-mode particles (diameters of 100-1000 nm) due to aqueous-phase

495   aerosol production. Other cloud processes include coagulation of cloud droplets with each other

496   and with interstitial aerosols (Hoose et al., 2008; Pierce et al., 2015). Our simulations include the

497   latter and aqueous-phase sulfate production. As clouds evaporate, cloud processing leads to

498   development of the 'Hoppel minima' of the MBL aerosol size distributions (Hoppel et al., 1987),

499   which the minimum aerosol diameter that activates to form a cloud droplet (about 50-70 nm for

500   the observations in Fig. 2). This minimum diameter is smallest in the winter transition (November

501   2015), suggesting that smaller particles activated under the very clean condition of this season

502   relative to the other seasons. As shown by Table 2, simulation noMSOA has an unacceptable

503   annual-mean MFE of 0.63, larger than the MFE of 0.23 for simulation BASE, which includes

504   particle growth due to MSOA.

505

506   The nature and flux of marine vapors forming MSOA are not well understood. As a result, we

507   developed a simplistic MSOA parameterization for use in this study, such that the MSOA

508   precursors vapor emissions are an increasing function of temperature. This approach yields a

509   seasonal cycle, and is in agreement with the temperature dependence trend found by previous

510   studies, including Meskhidze et al. (2015), Rodríguez-Ros et al. (2020a) and Rodríguez-Ros et al.,

511   2020b). However, future work is needed to examine the impact of this parameterization on the

512   simulated aerosol number, size and seasonal cycle in other ocean regions. We caution that the

513   current parameterization was developed for the NAAMES study region. We find that the simulated

514   NAAMES cruise-track median aerosol size distributions are sensitive to the coefficients used in

515   the parameterization ($S_{MSOA} = 70T - 350$ kg m^{-2} d^{-1}) (Supplemental Fig. S1 and Table S1). For

516   example, varying the temperature sensitivity between 50-100 and the intercept between 300-500

517   change the simulated number concentration of particles with diameters larger than 50 nm in the

518   MBL by up to a factor of two, with the greatest sensitivity during the summertime (Supplemental

519   Fig. S1). The vertical profiles also have a seasonally varying sensitivity of up to a factor of about

520   2 for aerosol number (N3, N10, and N3-N10), surface area, volume and OM on average in the

521   lowest 2 km of the atmosphere (Supplemental Figs. S2-4).

522

523   The near-surface campaign-median climax transition and declining phase OM concentrations are

524   within the 25th to 75th measurement percentiles for simulation BASE, and below the 25th percentile

525   of the observations for simulation noMSOA (Fig. 5). On average over the lowest 2 km of the

526   atmosphere during the May/June climax transition and August/September declining phase,

527   simulation BASE relative to noMSOA indicates that MSOA contributes about 200-400 ng m^{-3} to

528   simulated OM. Saliba et al. (submitted) suggest that MBL-measurement non-refractory OM during

529   NAAMES clean marine periods provides a good estimate of MSOA. Their seasonal-average non-

530   refractory OM of about 300-400 ng m^{-3} for the 2016 May/June climax transition and 2017

531   August/September declining phase is similar to our model result. The model-measurement

532   agreement for OM for 2017 is influenced by significant biomass burning with high altitude

533   emission injections during this time (Zheng et al., 2020b; Saliba et al., submitted). Errors in the

534   simulated emissions due to use of a GFED climatological-year emissions and injection-height

535   errors could account for some of the model-measurement bias at high altitudes. As well, despite

536   our implementation of a filter to remove measurement and model samples with strong in-plume

537   aerosol enhancements during times of high acetonitrile concentrations, some biomass burning

538   influence still affects the presented vertical profiles. Below 500 m altitude, condensing organic

539   vapors yielding MSOA also increase the simulated aerosol surface area and volume by a factor of

540   about 2-3 in all seasons (noMSOA versus BASE, Fig. 3), to be slightly over the 75th percentile of

541   the observations (Fig. 3). Surface area and volume results from the simulation are very sensitive

542   to the size-distribution simulation near the 282 nm diameter cut-off contributes to differences

543   between these simulations.

544

545   Figure 4 demonstrates that MSOA has a feedback on NPF. With lower aerosol surface area and

546   lower condensation sink (noMSOA), the N3 and N3-N10 below 2 km altitude are strongly

547   overpredicted because NPF increases and a lack of growth to larger sizes impacting N3-N10.

548   During November, the N3 and N3-N10 overprediction also occurs at altitudes above 2 km because

549   MSOA has a relatively greater influence on aerosol surface area at those altitudes in this season

550   (Fig. 3). In this less-polluted late fall season, the influence of MSOA is relatively stronger at higher

551   altitudes than in other seasons. Model-measurement agreement improves for N3 and N3-N10 with

552   the addition of MSOA (simulation BASE relative to noMSOA, Fig. 4). Kazil et al. (2011) also

553   found that condensing vapors generate a condensation sink that moderates the level of NPF in the

554   marine environment. As well, recent studies from the Arctic indicate a key contribution to particles

555   from condensing marine organic vapors (Burkart et al., 2017a; Willis et al., 2017; Croft et al.,

556   2019). The impact of MSOA on the simulated N10 vertical profiles is small. The cloud filtering,

557 which we applied to the model and measurement aerosol samples along the flight track,

558 preferentially removes some of the cloud-processed samples, and contributes to this result.

559

560 **3.4 Role of DMS**

561

562 Figure 2 shows that DMS also has a significant control on the simulated MBL aerosol size

563 distributions (BASE versus noDMS) for the four seasons of the NAAMES campaigns. The relative

564 impact of DMS is greatest during the times of greater marine biogenic activity (May/June climax

565 transition and August/September declining phase). Sulfuric acid from the oxidation of DMS has a

566 two-fold role in both NPF and in growing particles. However, as indicated by simulations

567 noABLNUC and noMSOA relative to BASE (Fig. 2), the DMS contribution is in concert with

568 both (1) a source of condensable marine organic vapors and (2) NPF near/above the MBL top. The

569 contribution of DMS to MBL particles is consistent with the findings of many previous studies,

570 including Chang et al. (2011), Ghahremaninezhad et al. (2016), Park et al. (2018), Sanchez et al.

571 (2018), Mahmood et al. (2019), Quinn et al. (2019) and Veres et al. (2020).

572

573 Simulation noABLNUC relative to noDMS for the marine-influenced MBL size distributions (Fig.

574 2) suggests that anthropogenic influences make a contribution as a source of particle-precursor

575 vapors for NPF, in addition to DMS. This relative contribution is particularly strong during the

576 accumulation phase (March/April 2018). In our simulations, anthropogenic SO_2 is oxidized to

577 H_2SO_4 and contributes to the particle precursors for NPF above/near the MBL top (in addition to

578 DMS oxidation products), followed by particle growth on descent into the MBL. As a result, Fig.

579 2 shows a greater underprediction of aerosol number for simulation noABLNUC versus noDMS.

580

581 Figure 6 indicates that the simulated DMS is generally consistent (within 10-50%) with the

582 observed DMS mixing ratio vertical profiles and their seasonal cycle for the NAAMES campaigns.

583 DMS makes the strongest contribution to simulated sulfate mass concentrations in the lowest 2 km

584 during the May/June climax transition, reducing model-measurement bias from about 40% to 10%

585 (Fig. 5). Figures 3 and 4 suggest that in the lowest 2 km of the atmosphere, DMS contributes to

586 both NPF and particle growth as there are increases in N3, N10, N3-N10, particle surface area and

587 volume for simulations BASE versus noDMS. However, this behavior is co-dependent on

588 conditions favorable to NPF near the MBL top and a source of MSOA.

589

590 **3.5 Role of ship traffic emissions**

591

592 Ship emissions are a source of primary and secondary particles, as well as a control on oxidants

593 (Corbett et al., 2010; Vinken et al., 2011; Holmes et al., 2014). Our simulations suggest that ship

594 emissions have a modest control on the NAAMES-region MBL marine-influenced aerosol size

595 distributions (Fig. 2, noSHIPS versus BASE), versus the factors discussed in the previous three

596 sub-sections. Ship emissions make about a 50% contribution to the simulated sulfate campaign-

597 median near-surface mass concentration in vertical profiles over the NAAMES study region (Fig.

598 5). For our simulations the impact of ship emissions on particle number is mostly limited to the

599 lowest 2 km. Simulation BASE relative to noSHIPS suggest that about 10% of the N10 in the

600 lowest 500 m of the atmosphere is attributed to ship emissions (Fig. 4). Figure 4 (right column)

601 indicates that among the four factors considered by our sensitivity studies, ship emissions have the

602 smallest influence on the NPF. Major trans-Atlantic ship traffic routes (Corbett et al. (2007) are

603 included in the NAMES study region. Enhancements in observed benzene mixing ratios in the

604 MBL (Fig. S5) relative to other long-lived tracers of anthropogenic emissions such as acetone (not

605 associated with ship traffic) (Fig. S6) are observational evidence that ship emissions influence the

606 study region.

607

608 Figure 6 demonstrates that atmospheric DMS mixing ratios are also sensitive to ship emissions.

609 This effect occurs because ship emissions are a control on oxidants in the MBL, and enhance OH

610 and NO_3, which are chemical sinks of DMS. As a result, simulated DMS mixing ratios increase

611 when ship emissions are removed. As ship traffic is expected to change in future years with

612 changes to routes and regulations (Gilgen et al., 2018; Bilsback et al. (submitted)), the relative

613 importance of ship emissions in the North Atlantic MBL will likely change.

614

615 **3.6 Radiative effects attributed to NPF near MBL top, MSOA, DMS and ship emissions**

616

617 Figure 7 shows the simulated two-monthly mean direct radiative effect (DRE) attributed to the

618 four factors we consider, (1) NPF near/above the MBL top, (2) MSOA, (3) DMS and (4) ship

619 emissions and magnitude of the regional-mean DREs over a region of the North Atlantic (40-60

620 °N, 20-50 °W). We note that the radiative effects attributed to the separate factors are not linearly

621 additive because the factors impact each other non-linearly. For example, turning off either MSOA

622 or nucleation above the boundary layer would shut down the majority of the production of

623 accumulation-mode particles in the MBL (Fig. 2) since these particles require both nucleation and

624 growth. Hence, adding the radiative effects from these two factors would result in double counting

625 some radiative effects.

626

627 The strongest DRE values attributed to the four considered factors are during the summer season

628 (climax transition (bloom maxima) and declining phase). This result highlights the link between

629 the level of marine biogenic activity and aerosol climate effects. Figure 7 indicates that the

630 strongest calculated DRE is attributed to condensing marine organic vapors, yielding MSOA. In

631 our simulations, MSOA contributes significantly to particle growth to diameters of about 100 to

632 200 nm, which can then interact directly with radiation (Fig. 2). This effect is greatest in the

633 declining phase because we used a temperature-dependent parameterization and sea surface

634 temperatures are warmest during the late summer. The DRE geographic distribution suggests an

635 increasing role for MSOA towards southern latitudes, again due to the temperature-dependent

636 parameterization. Further work is needed to examine the role of MSOA in the more southerly

637 latitudes as we cannot explicitly test this result across the annual cycle with the NAAMES

638 observations.

639

640 Among the factors considered, Figure 7 shows that during the time of the May/June phytoplankton

641 bloom, the aerosols produced and grown by the oxidation products of DMS have the second

642 strongest impact on the DRE, greatest over the regions where the bloom is located. This simulated

643 impact of DMS relies in part on (1) conditions favoring NPF processes above/near the MBL top,

644 and (2) growth by MSOA as the nascent DMS-related particles descend in the MBL.

645

646 The DRE attributed to the above/near-MBL-top NPF factor (Fig. 7, top row, ABLNUC) is

647 strongest in summertime, during the May/June climax transition (bloom maxima) and

648 August/September declining phase. Summertime is the season of the greatest photochemical

649 production of particle precursors for NPF. In order to contribute to the DRE, this NPF factor acts

650 in synergy with the other factors, particularly DMS as a source of particle precursors and MSOA

651 for particle growth, such that during the May/June climax transition season the DREs for those

652 factors dominate over the NPF factor (ABLNUC, Fig. 7).

653

654 The DREs for ship emissions have a similar geographic distribution as those for DMS. In these

655 regions, major international ship traffic routes are coincident with regions of higher biogenic

656 activity, enabling an interaction of biogenic and anthropogenic emissions. Ships enhance oxidant

657 levels, which promote formation of biogenic aerosol precursors such as sulfuric acid and MSA,

658 which arise from oxidation of DMS. Figure 6 shows that there is a ship-emission-related control

659 on atmospheric DMS mixing ratios, which increase when the ship-source oxidants are removed.

660 We caution that these DRE calculations should be viewed as an examination of the relative

661 contribution of the considered factors to climate effects in the North Atlantic. However, further

662 work is needed to gain confidence in the absolute magnitudes.

663

664 Figure 8 shows the calculated two-monthly mean cloud-albedo aerosol indirect effect (AIE)

665 attributed to each of the same four factors that we considered for the DREs. The AIEs are about

666 an order-of-magnitude larger than the calculated DRE for each respective factor. The AIE is

667 strongly controlled by changes to highly reflective MBL clouds, which are in turn very sensitive

668 to the aerosol number concentrations (diameters larger than about 50 to 70 nm that can act as

669 CCN), which are controlled by the MBL-related factors examined here. On the other hand, the

670 DRE is relatively more sensitive to aerosol abundance in mid-tropospheric layers, which are less

671 influenced by the considered processes.

672

673 The strongest simulated AIEs for all considered factors are during the May/June climax transition

674 (Fig. 8). There is a strong synergy among all factors that reach their maxima during May/June

675 when the effective combination of sources, photochemistry and particle production/growth

676 processes peak. As well, during summertime, the magnitude of the AIE for all factors is greater in

677 the more northward regions of the North Atlantic relative to more southerly latitudes. These more

678 northerly regions are less influenced by continental pollution and have lower CCN concentrations,

679   coupled with persistent low cloud cover. These conditions make these regions quite sensitive to

680   the factors controlling MBL aerosol size distributions studied here.

681

682   In all seasons, we calculated a stronger AIE related to (1) NPF near/above the MBL top (ABLNUC,

683   top row, Fig. 8) and (2) MSOA (contributor to particle growth) than to (1) DMS and (2) ship

684   emissions. In our simulations, the major source of CCN-sized particles in the North Atlantic MBL

685   during the summer is particle nucleation near/above the MBL top with growth by MSOA. Without

686   either of these factors, the number concentration of CCN-sized particles in the simulations drops

687   dramatically (Fig. 2). Hence, it is unsurprising that the largest simulated AIEs are due to these two

688   factors during the summertime (climate transition and declining phase). The stronger AIEs

689   attributed to NPF near/above the MBL top (Fig. 8, top row, ABLNUC) relative to DMS and ship

690   emissions indicate that near/above-MBL NPF in our simulations is controlled not only by the

691   sulfuric acid from the oxidation of DMS or ship SO_2, but also arising from other sources, including

692   SO_2 transported from continental sources. However, the maximum North Atlantic regional-mean

693   AIE attributed to ship emissions (-0.62 W m^{-2} for the May/June climax transition) still exceeds the

694   global mean effect of -0.155 W m^{-2} attributed to international shipping calculated by Jin et al.

695   (2018), showing the strong location-dependence and seasonality of this factor.

696

697   Similar to the DRE, we consider that these AIE calculations indicate the relative importance of the

698   considered factors, further work is needed to gain confidence in the absolute magnitudes. Like the

699   DRE estimates, the separate AIEs are not linearly additive. Other aerosol indirect effects related

700   to changes in cloud lifetime and precipitation are the subject of future work. In summary, these

701   calculated DREs and AIEs suggest that aerosol-climate impacts for North Atlantic regions are

702   controlled by a combination of strong biogenic and anthropogenic influences and that the

703   nucleation near/above the MBL top contributes to important radiative effects.

704

705   **4. Conclusions**

706

707   In this study, we examined aerosol size distribution and composition measurements from the

708   NAAMES campaigns. These ship and aircraft campaigns took place over four separate stages of

709   the annual cycle of marine biogenic activity in the Northwest Atlantic during 2015-2018. We used

710   the GEOS-Chem-TOMAS model with size-resolved aerosol microphysics to interpret these

711   NAAMES measurements. Observations showed enhancements in total aerosol number

712   concentrations (diameters between 3-10 nm, as well as greater than 3 and 10 nm) and variability

713   near 1 km altitude, indicative of new particle formation and most pronounced during the May/June

714   2016 climax transition (phytoplankton bloom maxima). The November 2015 winter transition

715   (phytoplankton bloom minima) was characterized by the lowest particle number concentrations.

716   During the summer months, OM, followed by sulfate mass concentrations dominated the total

717   aerosol loading in the lowest 2 km. Peak near-surface sulfate concentrations occurred in May/June

718   during the phytoplankton bloom, whereas peak near-surface OM concentrations were in

719   August/September. Campaign-median MBL aerosol size distributions were dominated by Aitken

720   mode particles (diameters 10-100 nm) during the summertime (May/June climax transition and

721   August/September declining phase). The larger accumulation mode particles were dominant in the

722   November winter transition and March/April accumulation phase.

723

724   Our simulations suggested that a synergy of key factors contributed to Northwest Atlantic MBL

725   aerosol size distributions, including (1) new particle formation (NPF) near/above the MBL top, (2)

726   growth of the newly formed particles by condensation of marine organic vapors, forming marine

727   secondary organic aerosol (MSOA), which yields more abundant CCN-sized particles that descend

728   into the MBL while continuing to grow and being subject to cloud processing (e.g. aqueous-phase

729   aerosol production, which does not add to particle number), (3) DMS-oxidation products that

730   contribute to particle formation and growth, and (4) ship emissions, which are a source of primary

731   and secondary particles and also contribute to atmospheric oxidants. These findings are in

732   agreement with previous observational-based studies for the North Atlantic region (e.g. Sanchez

733   et al., 2018; Zheng et al., 2020)

734

735   We calculated the aerosol direct (DRE) and cloud-albedo indirect (AIE) radiative effects over the

736   North Atlantic attributed to four key factors controlling MBL aerosols. The cooling effects were

737   about a factor of 10 larger for the AIEs than the respective DREs. The strong AIE response was

738   attributed to the strong sensitivity of the MBL cloud reflectivity to the MBL-related factors that

739   we examined. Mid-tropospheric aerosol (altitude of transport of continental pollution) has a strong

740   impact on the DRE and the factors that we considered had less impact at these altitudes. The

741   maximum regional-mean (40-60 °N, 20-50 °W) DRE for our simulations was -0.26 W m^{-2}, for the

742   August/September declining phase. This DRE was connected to the temperature-dependent source

743   of MSOA, which had a key role in growing simulated particles to large enough (diameters of 100-

744   200 nm) to strongly reflect incoming solar radiation. The maximum AIE was -3.37 W m^{-2}, for the

745   May/June climax transition phase (peak phytoplankton bloom). This AIE was related to the role

746   MSOA in growing new particles to CCN sizes as they descend into the MBL and are subject to

747   further growth in clouds after their formation near the MBL top. The AIE attributed to the NPF

748   factor was nearly as large (-2.27 W m^{-2}) during May/June. The NPF and MSOA factors act in

749   concert with each other and removal of either of these factors contributed to shutdown the

750   production of cloud-condensation-nuclei-size particles.

751

752   This study highlighted the importance of processes connected to both marine biogenic activity and

753   anthropogenic activity in controlling aerosol size distributions in the Northwest Atlantic MBL. We

754   identified key factors, which could be the focus of future work. Particularly, work is needed to

755   better understand the nature, flux, and chemistry of marine organic vapors that can form MSOA.

756   As well, work is needed to better understand the contributors to NPF near and above the MBL top.

757   Further work is also needed to understand the interactions of the considered factors with cloud

758   processing of aerosols and its relative importance in particle growth. As the Earth's climate

759   changes and shipping traffic/regulations/routes change, work to understand the source strength of

760   DMS, MSOA, and shipping emissions is highly relevant. Such work will bridge the knowledge

761   gaps related to factors controlling aerosols in the marine MBL and their climate impacts.

762

763   **Code and data availability.** The NAAMES project website is at https://naames.larc.nasa.gov. The

764   NAAMES airborne and ship datasets used in this paper are publicly available and permanently

765   archived in the NASA Atmospheric Science Data Center (ASDC;

766   https://doi.org/10.5067/Suborbital/NAAMES/DATA001) and the SeaWiFS Bio-Optical Archive

767   and Storage System (SeaBASS; https://doi.org/10.5067/SeaBASS/NAAMES/DATA001). The

768   ship datasets generated during and analyzed for NAAMES studies are also available in the UCSD

769   Library Digital Collection repository, https://doi.org/10.6075/J04T6GJ6. The GEOS-Chem model

770   is freely available for download at https://github.com/geoschem/geos-chem (last access 19 July

771   2020).

772

773 **Supplement link.**

774

775 **Author contributions.** BC, RVM and JRP designed the study. BC conducted the GEOS-Chem-
776 TOMAS simulations, led the related analysis, and wrote the manuscript with contributions from
777 all coauthors. RHM, ECC, and LDZ contributed the aerosol measurements from aboard the NASA
778 C130 aircraft. AW, MM and AS contributed the gas-phase measurements from aboard the NASA
779 C130 aircraft. LMR and GS contributed the aerosol measurements from aboard the R/V Atlantis.
780 RYWC and HL contributed to the interpretation of model-measurement comparisons. EEM
781 contributed the CEDS data set. KRB contributed to the off-line radiative calculations, MG
782 contributed the satellite DMS data set.

783

784 **Competing interests.** The authors declare that they have no conflict of interest.

785

786 **Acknowledgements**. BC, RVM and RYWC acknowledge research funding provided by the
787 Ocean Frontier Institute, through an award from the Canada First Research Excellence Fund.
788 JRP and KRB acknowledge funding support from the Monfort Excellence Fund, and the US
789 Department of Energy's Atmospheric System Research, an Office of Science, Office of
790 Biological and Environmental Research program, under grant DE-SC0019000. LMR and GS
791 acknowledge funding support from NASA grant NNX15AE66G. RHM, ECC, LDZ, LMR, and
792 GS acknowledge funding support from the NASA NAAMES EVS-2 project. HL acknowledges
793 funding support from the NASA NAAMES mission and the National Institute of Aerospace's
794 IRAD program. DMS measurements aboard the NASA C-130 during NAAMES were supported
795 by the Austrian Federal Ministry for Transport, Innovation and Technology (bmvit) through the
796 Austrian Space Applications Programme (ASAP) of the Austrian Research Promotion Agency
797 (FFG). MM's participation in NAAMES 2016 was funded by the Tiroler Wissenschaftsfonds
798 (grant # UNI-0404/1895). AS's participation in NAAMES 2017 was partly funded by National
799 Institute of Aerospace (Task No 80LARC18F0031). MG acknowledges funding support from the
800 Natural Sciences and Engineering Research Council of Canada through the NETCARE project
801 of the Climate Change and Atmospheric Research Program. Tomas Mikoviny is acknowledged
802 for technical support; Ionicon Analytik is acknowledged for instrumental support

803

804   **References**.

805

806   Abbatt, J. P. D., Leaitch, W. R., Aliabadi, A. A., Bertram, A. K., Blanchet, J.-P., Boivin-Rioux,
807   A., Bozem, H., Burkart, J., Chang, R. Y. W., Charette, J., Chaubey, J. P.,
808   Christensen, R. J., Cirisan, A., Collins, D. B., Croft, B., Dionne, J., Evans, G. J.,
809   Fletcher, C. G., Galí, M., Ghahremaninezhad, R., Girard, E., Gong, W., Gosselin,
810   M., Gourdal, M., Hanna, S. J., Hayashida, H., Herber, A. B., Hesaraki, S., Hoor, P.,
811   Huang, L., Hussherr, R., Irish, V. E., Keita, S. A., Kodros, J. K., Köllner, F.,
812   Kolonjari, F., Kunkel, D., Ladino, L. A., Law, K., Levasseur, M., Libois, Q.,
813   Liggio, J., Lizotte, M., Macdonald, K. M., Mahmood, R., Martin, R. V., Mason, R.
814   H., Miller, L. A., Moravek, A., Mortenson, E., Mungall, E. L., Murphy, J. G.,
815   Namazi, M., Norman, A.-L., O'Neill, N. T., Pierce, J. R., Russell, L. M., Schneider,
816   J., Schulz, H., Sharma, S., Si, M., Staebler, R. M., Steiner, N. S., Thomas, J. L., von
817   Salzen, K., Wentzell, J. J. B., Willis, M. D., Wentworth, G. R., Xu, J.-W., and
818   Yakobi-Hancock, J. D.: Overview paper: New insights into aerosol and climate in
819   the Arctic, Atmos. Chem. Phys., 19, 2527–2560, https://doi.org/10.5194/acp-19-
820   2527-2019, 2019.

821   Abdul-Razzak, H. and Ghan, S. J.: A parameterization of aerosol activation 3. Sectional
822   representation, J. Geophys. Res., 107, 4026, doi:10.1029/2001JD000483, 2002.

823   Adams, P. J. and Seinfeld, J. H.: Predicting global aerosol size distributions in general circulation
824   models, J. Geophys. Res., 107, 4370, doi:10.1029/2001JD001010, 2002.

825   Allan, J. D., Williams, P. I., Najera, J., Whitehead, J. D., Flynn, M. J., Taylor, J. W., Liu, D.,
826   Darbyshire, E., Carpenter, L. J., Chance, R., Andrews, S. J., Hackenberg, S. C. and
827   McFiggans, G.: Iodine observed in new particle formation events in the Arctic
828   atmosphere during ACCACIA, Atmos. Chem. Phys., 15(10), 5599–5609,
829   doi:10.5194/acp-15-5599-2015, 2015.

830   Amos, H. M., Jacob, D. J., Holmes, C. D., Fisher, J. A., Wang, Q., Yantosca, R. M., Corbitt, E. S.,
831   Galarneau, E., Rutter, A. P., Gustin, M. S., Steffen, A., Schauer, J. J., Graydon, J.
832   A., St Louis, V. L., Talbot, R. W., Edgerton, E. S., Zhang, Y. and Sunderland, E.
833   M.: Gas-particle partitioning of atmospheric Hg(II) and its effect on global mercury

834   deposition, Atmos. Chem. Phys., 12(1), 591–603, doi:10.5194/acp-12-591-2012,
835   2012.

836   Ault, A. P., Moffet, R. C., Baltrusaitis, J., Collins, D. B., Ruppel, M. J., Cuadra-Rodriguez, L. A.,
837   Zhao, D., Guasco, T. L., Ebben, C. J., Geiger, F. M., Bertram, T. H., Prather, K. A.
838   and Grassian, V. H.: Size-Dependent Changes in Sea Spray Aerosol Composition
839   and Properties with Different Seawater Conditions, Environ. Sci. Technol., 47(11),
840   5603–5612, doi:10.1021/es400416g, 2013.

841   Barnes, I., Hjorth, J. and Mihalapoulos, N.: Dimethyl sulfide and dimethyl sulfoxide and their
842   oxidation   in   the   atmosphere,   Chem.   Rev.,   106(3),   940–975,
843   doi:10.1021/cr020529+, 2006.

844   Bates, T. S., Coffman, D. J., Covert, D. S., Quinn, P. K.: Regional marine boundary layer aerosol
845   size distributions in the Indian, Atlantic, and Pacific Oceans: A comparison of
846   INDOEX measurements with ACE-1, ACE-2, and Aerosols99. J. Geophys. Res.
847   Atmos., 107, D19, doi:10.1029/2001JD001174, 2002.

848   Bates, T. S., Quinn, P. K., Coffman, D. J., Johnson, J. E., Upchurch, L., Saliba, G. and Lewis, S.:
849   Variability in Marine Plankton Ecosystems Are Not Observed in Freshly Emitted
850   Sea Spray Aerosol Over the North Atlantic Ocean, Geophys. Res. Lett.,
851   doi:10.1029/2019GL085938, 2020.

852   Behrenfeld, M. J., Moore, R. H., Hostetler, C. A., Graff, J., Gaube, P., Russell, L. M., Chen, G.,
853   Doney, S. C., Giovannoni, S., Liu, H., Proctor, C., Bolaños, L. M., Baetge, N.,
854   Davie-Martin, C., Westberry, T. K., Bates, T. S., Bell, T. G., Bidle, K. D., Boss, E.
855   S., Brooks, S. D., Cairns, B., Carlson, C., Halsey, K., Harvey, E. L., Hu, C., Karp-
856   Boss, L., Kleb, M., Menden-Deuer, S., Morison, F., Quinn, P. K., Scarino, A. J.,
857   Anderson, B., Chowdhary, J., Crosbie, E., Ferrare, R., Hair, J. W., Hu, Y., Janz, S.,
858   Redemann, J., Saltzman, E., Shook, M., Siegel, D. A., Wisthaler, A., Martin, M. Y.
859   and Ziemba, L.: The North Atlantic Aerosol and Marine Ecosystem Study
860   (NAAMES): Science Motive and Mission Overview, Front. Mar. Sci., 6, 122,
861   doi:10.3389/fmars.2019.00122, 2019.

862   Bilsback, K., Kerry, D., Croft, B., Ford, B., Carter, E., Martin, R. V., and Pierce, J. R.: Beyond
863   SO_2 reductions from shipping: Assessing the impact of NOx and carbonaceous

864   particle controls on human health and climate, Environ. Res. Lett., (in review),
865   2020).

866 Boucher, O. and Haywood, J.: Estimates of the Direct and Indirect Radiative Forcing Due to
867   Tropospheric Aerosols: A Review, Rev. Geophys., 34(4), 513–543, 2000.

868 Boylan, J. W. and Russell, A. G.: PM and light extinction model performance metrics, goals, and
869   criteria for three-dimensional air quality models, Atmos. Environ., 40(26), 4946–
870   4959, doi:10.1016/j.atmosenv.2005.09.087, 2006.

871 Brooks, S. D. and Thornton, D. C. O.: Marine Aerosols and Clouds, Ann. Rev. Mar. Sci., 10(1),
872   289–313, doi:10.1146/annurev-marine-121916-063148, 2018.

873 Browse, J., Carslaw, K. S., Arnold, S. R., Pringle, K. and Boucher, O.: The scavenging processes
874   controlling the seasonal cycle in Arctic sulphate and black carbon aerosol, Atmos.
875   Chem. Phys., 12(15), 6775–6798, doi:10.5194/acp-12-6775-2012, 2012.

876 Brüggemann, M., Hayeck, N. and George, C.: Interfacial photochemistry at the ocean surface is a
877   global source of organic vapors and aerosols, Nat. Commun., 1–8,
878   doi:10.1038/s41467-018-04528-7, 2018.

879 Burkart, J., Hodshire, A. L., Mungall, E. L., Pierce, J. R., Collins, D. B., Ladino, L. A., Lee, A. K.
880   Y., Irish, V., Wentzell, J. J. B., Liggio, J., Papakyriakou, T., Murphy, J. and Abbatt,
881   J.: Organic Condensation and Particle Growth to CCN Sizes in the Summertime
882   Marine Arctic Is Driven by Materials More Semivolatile Than at Continental Sites,
883   Geophys. Res. Lett., 44(20), 10,725-10,734, doi:10.1002/2017GL075671, 2017a.

884 Burkart, J., Willis, M. D., Bozem, H., Thomas, J. L., Law, K., Hoor, P., Aliabadi, A. A., Köllner,
885   F., Schneider, J., Herber, A., Abbatt, J. P. D. and Leaitch, W. R.: Summertime
886   observations of elevated levels of ultrafine particles in the high Arctic marine
887   boundary layer, Atmos. Chem. Phys., 17(8), 5515–5535, doi:10.5194/acp-17-5515-
888   2017, 2017b.

889 Carpenter, L. J. and Nightingale, P. D.: Chemistry and Release of Gases from the Surface Ocean,
890   Chem. Rev., 115(10), 4015–4034, doi:10.1021/cr5007123, 2015.

891 Carpenter, L. J., Archer, S. D. and Beale, R.: Ocean-atmosphere trace gas exchange, Chem. Soc.
892   Rev., 41(19), 6473–6506, doi:10.1039/c2cs35121h, 2012.

893 Carslaw, K. S., Boucher, O., Spracklen, D. V., Mann, G. W., Rae, J. G. L., Woodward, S., and
894   Kulmala, M.: A review of natural aerosol interactions and feedbacks within the

895   Earth system, Atmos. Chem. Phys., 10, 1701–1737, https://doi.org/10.5194/acp-
896   10-1701-2010, 2010.

897   Carslaw, K. S., Lee, L. A., Reddington, C. L., Pringle, K. J., Rap, A., Forster, P. M., Mann, G. W.,
898   Spracklen, D. V, Woodhouse, M. T., Regayre, L. A. and Pierce, J. R.: Large
899   contribution of natural aerosols to uncertainty in indirect forcing, Nature, 503, 67
900   [online] Available from: http://dx.doi.org/10.1038/nature12674, 2013.

901   Cavalli, F., Facchini, M. C., Decesari, S., Mircea, M., Emblico, L., Fuzzi, S., Ceburnis, D., Yoon,
902   Y. J., O'Dowd, C., Putaud, J. P. and Dell'Acqua, A.: Advances in characterization
903   of size-resolved organic matter in marine aerosol over the North Atlantic, J.
904   Geophys. Res. D Atmos., 109(24), 1–14, doi:10.1029/2004JD005137, 2004.

905   Ceburnis, D., O'Dowd, C., Jennings, G. S., Facchini, M. C., Emblico, L., Decesari, S., Fuzzi, S.
906   and Sakalys, J.: Marine aerosol chemistry gradients : Elucidating primary and
907   secondary processes and fluxes, Geophys. Res. Lett., 35(2), 1–5,
908   doi:10.1029/2008GL033462, 2008.

909   Chang, R. Y. W., Sjostedt, S. J., Pierce, J. R., Papakyriakou, T. N., Scarratt, M. G., Michaud, S.,
910   Levasseur, M., Leaitch, W. R. and Abbatt, J. P. D.: Relating atmospheric and
911   oceanic DMS levels to particle nucleation events in the Canadian Arctic, J.
912   Geophys. Res. Atmos., 116(21), 1–10, doi:10.1029/2011JD015926, 2011.

913   Charlson, R. J., Lovelock, J. E., Andreae, M. O. and Warren, S. G.: Oceanic phytoplankton,
914   atmospheric sulphur, cloud albedo and climate, Nature, 326(6114), 655–661,
915   doi:10.1038/326655a0, 1987.

916   Charlson, R. J., Schwartz, S. E., Hales, J. M., Cess, R. D., Coakley, J. A., Hansen, J. E. and
917   Hofmann, D. J.: Climate Forcing by Anthropogenic Aerosols, Science (80),
918   255(5043),   423–430   [online]   Available   from:
919   http://science.sciencemag.org/content/255/5043/423.abstract, 1992.

920   Chen, H., Varner, M. E., Gerber, R. B. and Finlayson-Pitts, B. J.: Reactions of Methanesulfonic
921   Acid with Amines and Ammonia as a Source of New Particles in Air, J. Phys.
922   Chem. B, 120(8), 1526–1536, doi:10.1021/acs.jpcb.5b07433, 2016.

923   Chen, Q., Sherwen, T., Evans, M. and Alexander, B.: DMS oxidation and sulfur aerosol formation
924   in the marine troposphere : a focus on reactive halogen and multiphase chemistry,
925   Atmos. Chem. Phys., 18, 13617–13637, 2018.

926   Chen, Y.-C., Christensen, M. W., Stephens, G. L. and Seinfeld, J. H.: Satellite-based estimate of
927   global aerosol–cloud radiative forcing by marine warm clouds, Nat. Geosci., 7(9),
928   643–646, doi:10.1038/ngeo2214, 2014.

929   Collins, D. B., Burkart, J., Chang, R. Y.-W., Lizotte, M., Boivin-Rioux, A., Blais, M., Mungall, E.
930   L., Boyer, M., Irish, V. E., Massé, G., Kunkel, D., Tremblay, J.-É., Papakyriakou,
931   T., Bertram, A. K., Bozem, H., Gosselin, M., Levasseur, M., and Abbatt, J. P. D.:
932   Frequent ultrafine particle formation and growth in Canadian Arctic marine and
933   coastal environments, Atmos. Chem. Phys., 17, 13119–13138,
934   https://doi.org/10.5194/acp-17-13119-2017, 2017.

935   Corbett, J. J., Winebrake, J. J., Green, E. H., Kasibhatla, P., Eyring, V. and Lauer, A.: Mortality
936   from Ship Emissions: A Global Assessment, Environ. Sci. Technol., 41(24), 8512–
937   8518, doi:10.1021/es071686z, 2007.

938   Corbett, J. J., Lack, D. A., Winebrake, J. J., Harder, S., Silberman, J. A., and Gold, M.: Arctic
939   shipping emissions inventories and future scenarios, Atmos. Chem. Phys., 10,
940   9689–9704, https://doi.org/10.5194/acp-10-9689-2010, 2010.

941   Cravigan, L. T., Ristovski, Z., Modini, R. L., Keywood, M. D., and Gras, J. L.: Observation of
942   sea-salt fraction in sub-100 nm diameter particles at Cape Grim, J. Geophys. Res.
943   Atmos., 120, 1848–1864, doi:10.1002/2014JD022601, 2015

944   Cravigan, L. T., Mallet, M. D., Vaattovaara, P., Harvey, M. J., Law, C. S., Modini, R. L., Russell,
945   L. M., Stelcer, E., Cohen, D. D., Olsen, G., Safi, K., Burrell, T. J. and Ristovski,
946   Z.: Sea spray aerosol organic enrichment , water uptake and surface tension effects,
947   Atmos. Chem. Phys., 20, 7955–7977, https://doi.org/10.5194/acp-20-7955-2020,
948   2020.

949   Croft, B., Wentworth, G. R., Martin, R. V, Leaitch, W. R., Murphy, J. G., Murphy, B. N., Kodros,
950   J. K., Abbatt, J. P. D. and Pierce, J. R.: Contribution of Arctic seabird-colony
951   ammonia to atmospheric particles and cloud-albedo radiative effect, Nat.
952   Commun., 7, 13444, doi:10.1038/ncomms13444, 2016a.

953   Croft, B., Martin, R. V., Richard Leaitch, W., Tunved, P., Breider, T. J., D'Andrea, S. D. and
954   Pierce, J. R.: Processes controlling the annual cycle of Arctic aerosol number and
955   size distributions, Atmos. Chem. Phys., 16(6), 3665–3682, doi:10.5194/acp-16-
956   3665-2016, 2016b.

957   Croft, B., Martin, R. V., Leaitch, W. R., Burkart, J., Chang, R. Y.-W., Collins, D. B., Hayes, P. L.,
958   Hodshire, A. L., Huang, L., Kodros, J. K., Moravek, A., Mungall, E. L., Murphy,
959   J. G., Sharma, S., Tremblay, S., Wentworth, G. R., Willis, M. D., Abbatt, J. P. D.
960   and Pierce, J. R.: Arctic marine secondary organic aerosol contributes significantly
961   to summertime particle size distributions in the Canadian Arctic Archipelago,
962   Atmos. Chem. Phys., 19(5), 2787–2812, doi:10.5194/acp-19-2787-2019, 2019.

963   Cui, T., Green, H. S., Selleck, P. W., Zhang, Z., Brien, R. E. O., Gold, A., Keywood, M., Kroll, J.
964   H. and Surratt, J. D.: Chemical Characterization of Isoprene- and Monoterpene-
965   Derived Secondary Organic Aerosol Tracers in Remote Marine Aerosols over a
966   Quarter Century, doi:10.1021/acsearthspacechem.9b00061, 2019.

967   Dall´Osto, M., Simo, R., Harrison, R. M., Beddows, D. C. S., Saiz-Lopez, A., Lange, R., Skov,
968   H., Nøjgaard, J. K., Nielsen, I. E. and Massling, A.: Abiotic and biotic sources
969   influencing spring new particle formation in North East Greenland, Atmos.
970   Environ., 190(July), 126–134, doi:10.1016/J.ATMOSENV.2018.07.019, 2018.

971   DeCarlo, P. F., Kimmel, J. R., Trimborn, A., Northway, M. J., Jayne, J. T., Aiken, A. C., Gonin,
972   M., Fuhrer, K., Horvath, T., Docherty, K. S., Worsnop, D. R., and Jimenez, J. L.:
973   Field-deployable, high-resolution, time-of-flight aerosol mass spectrometer,
974   Analytical Chemistry 78, (24), 8281-8289, 2006.

975   Decesari, S., Finessi, E., Rinaldi, M., Paglione, M., Fuzzi, S., Stephanou, E. G., Tziaras, T., Spyros,
976   A., Ceburnis, D., O'Dowd, C., Osto, M. D., Harrison, R. M., Allan, J., Coe, H. and
977   Facchini, M. C.: Primary and secondary marine organic aerosols over the North
978   Atlantic Ocean during the MAP experiment, J. Geophys. Res., 116, D22210, 1–21,
979   doi:10.1029/2011JD016204, 2011.

980   de Leeuw, G., Andreas, E. L., Anguelova, M. D., Fairall, C. W., Lewis, E. R., O'Dowd, C., Schulz,
981   M., and Schwartz, S. E.: Production flux of sea spray aerosol, Rev. Geophys., 49,
982   RG2001, https://doi.org/10.1029/2010RG000349, 2011.

983   DeMott, P. J., Hill, T. C. J., McCluskey, C. S., Prather, K. A., Collins, D. B., Sullivan, R. C.,
984   Ruppel, M. J., Mason, R. H., Irish, V. E. and Lee, T.: Sea spray aerosol as a unique
985   source of ice nucleating particles, Proc. Natl. Acad. Sci., 113(21), 5797–5803
986   [online] Available from: http://www.pnas.org/content/113/21/5797.full.pdf, 2016.

987   EC-JRC/PBL: Emission Database for Global Atmospheric Research (EDGAR), release EDGAR
988   v4.2 FT2012, http://edgar.jrc.ec.europa.eu (last access: 15 January 2018), 2012.

989   Facchini, M. C., Decesari, S., Rinaldi, M., Carbone, C., Finessi, E., Mircea, M., Fuzzi, S., Moretti,
990   F., Tagliavini, E., Ceburnis, D. and O'Dowd, C.: Important Source of Marine
991   Secondary Organic Aerosol from Biogenic Amines, Environ. Sci. Technol., 42(24),
992   9116–9121, doi:10.1021/es8018385, 2008.

993   Fast, J. D., Berg, L. K., Zhang, K., Easter, R. C., Ferrare, R. A., Hair, J. W., Hostetler, C. A., Liu,
994   Y., Ortega, I., Sedlacek III, A., Shilling, J. E., Shrivastava, M., Springston, S. T.,
995   Tomlinson, Jason, M., Rainer, V., Wilson, J., Zaveri, R. A. and Zelenyuk, A.:
996   Model representations of aerosol layers transported from North America over the
997   Atlantic Ocean during the Two-Column Aerosol Project, J. Geophys. Res. Atmos.,
998   121, 9814–9848, doi:10.1002/2016JD025248, 2016.

999   Fiddes, S. L., Woodhouse, M. T., Nicholls, Z., Lane, T. P. and Schofield, R.: Cloud, precipitation
1000   and radiation responses to large perturbations in global dimethyl sulfide, Atmos.
1001   Chem. Phys., 18, 10177–10198, https://doi.org/10.5194/acp-18-10177-2018, 2018.

1002 Fisher, J. A., Jacob, D. J., Purdy, M. T., Kopacz, M., Le Sager, P., Carouge, C., Holmes, C. D.,
1003   Yantosca, R. M., Batchelor, R. L., Strong, K., Diskin, G. S., Fuelberg, H. E.,
1004   Holloway, J. S., Hyer, E. J., McMillan, W. W., Warner, J., Streets, D. G., Zhang,
1005   Q., Wang, Y. and Wu, S.: Source attribution and interannual variability of Arctic
1006   pollution in spring constrained by aircraft (ARCTAS, ARCPAC) and satellite
1007   (AIRS) observations of carbon monoxide, Atmos. Chem. Phys., 10(3), 977–996,
1008   doi:10.5194/acp-10-977-2010, 2010.

1009 Fossum, K.N., Ovadnevaite, J., Ceburnis, D. Preißler, J., Snider, J. R., Huang, R. J., Zuend, A. and
1010   O'Dowd, C.: Sea-spray regulates sulfate cloud droplet activation over oceans, NPJ
1011   Clim. Atmos. Sci., 3, 14, https://doi.org/10.1038/s41612-020-0116-2, 2020.

1012 Galí, M., and Simó, R.: A meta-analysis of oceanic DMS and DMSP cycling processes:
1013   Disentangling the summer paradox, Global Biogeochem. Cycles, 29, 496–515,
1014   doi:10.1002/2014GB004940, 2015.

1015 Galí, M., Levasseur, M., Devred, E., Simó, R. and Babin, M.: Sea-surface dimethylsulfide (DMS)
1016   concentration from satellite data at global and regional scales, Biogeosciences, 15,
1017   3497–3519, https://doi.org/10.5194/bg-15-3497-2018, 2018.

1018 Galí, M., Devred, E., Babin, M. and Levasseur, M.: Decadal increase in Arctic dimethylsulfide
1019   emission, Proc. Natl. Acad. Sci., 116(39), 19311–19317,
1020   doi:10.1073/pnas.1904378116, 2019.
1021 Gantt, B. and Meskhidze, N.: The physical and chemical characteristics of marine primary organic
1022   aerosol: A review, Atmos. Chem. Phys., 13(8), 3979–3996, doi:10.5194/acp-13-
1023   3979-2013, 2013.
1024 Ghahremaninezhad, R., Norman, A. L., Abbatt, J. P. D., Levasseur, M. and Thomas, J. L.:
1025   Biogenic, anthropogenic and sea salt sulfate size-segregated aerosols in the Arctic
1026   summer, Atmos. Chem. Phys., 16(8), 5191–5202, doi:10.5194/acp-16-5191-2016,
1027   2016.
1028 Ghahremaninezhad, R., Gong, W., Galí, M., Norman, A., Beagley, S. R., Akingunola, A., Zheng,
1029   Q., Lupu, A., Lizotte, M., Levasseur, M. and Leaitch, W. R.: Dimethyl sulfide and
1030   its role in aerosol formation and growth in the Arctic summer – a modelling study,
1031   Atmos. Chem. Phys., 19, 14455–14476, https://doi.org/10.5194/acp-19-14455-
1032   2019, 2019.
1033 Gilgen, A., Ting, W., Huang, K., Ickes, L., Neubauer, D. and Lohmann, U.: How important are
1034   future marine and shipping aerosol emissions in a warming Arctic summer and
1035   autumn ?, Atmos. Chem. Phys., 18, 10521–10555, https://doi.org/10.5194/acp-18-
1036   10521-2018, 2018.
1037 Grassian, V. H., Quinn, P. K., Collins, D. B., Bates, T. S. and Prather, K. A.: Chemistry and Related
1038   Properties of Freshly Emitted Sea Spray Aerosol, Chem. Rev., 115(10), 4383–
1039   4399, doi:10.1021/cr500713g, 2015.
1040 Hamacher-Barth, E., Leck, C. and Jansson, K.: Size-resolved morphological properties of the high
1041   Arctic summer aerosol during ASCOS-2008, Atmos. Chem. Phys., 16, 6577–6593,
1042   doi:10.5194/acp-16-6577-2016, 2016.
1043 Hodshire, A. L., Campuzano-jost, P., Kodros, J. K., Croft, B., Nault, B. A., Schroder, J. C.,
1044   Jimenez, J. L. and Pierce, J. R.: The potential role of methanesulfonic acid (MSA
1045   ) in aerosol formation and growth and the associated radiative forcings, Atmos.
1046   Chem. Phys., 19, 3137-3160, https://doi.org/10.5194/acp-19-3137-2019 , 2019.
1047 Hoesly, R. M., Smith, S. J., Feng, L., Klimont, Z., Janssens-Maenhout, G., Pitkanen, T., Seibert,
1048   J. J., Vu, L., Andres, R. J., 1010 Bolt, R. M., Bond, T. C., Dawidowski, L., Kholod,

1049 N., Kurokawa, J. I., Li, M., Liu, L., Lu, Z., Moura, M. C. P., O'Rourke, P. R., and
1050 Zhang, Q.: Historical (1750–2014) anthropogenic emissions of reactive gases and
1051 aerosols from the Community Emissions Data System (CEDS), Geosci. Model
1052 Dev., 11, 369-408, 10.5194/gmd-11-369-2018, 2018.

1053 Hoffman, E. H., Tilgner, A., Schrödner, R., Bräuer, P., Wolke, R. and Herrmann, H.: An advanced
1054 modeling study on the impacts and atmospheric implications of multiphase
1055 dimethyl sulfide chemistry, Proc. Natl., Acad. Sci., 113, (42), 11776-11781,
1056 https://doi.org/10.1073/pnas.1606320113, 2016.

1057 Holmes, C. D., Prather, M. J. and Vinken, G. C. M.: The climate impact of ship NO x emissions :
1058 an improved estimate accounting for plume chemistry, Atmos. Chem. Phys., 14,
1059 6801–6812, doi:10.5194/acp-14-6801-2014, 2014.

1060 Hoose, C., Lohmann, U., Bennartz, R., Croft, B., Lesins, G.: Global simulations of aerosol
1061 processing in clouds, Atmos. Chem. Phus., 8, 6939–6963, 2008.

1062 Hoppel, W. A., G. M. Frick, and R. E. Larson (1986), Effect of nonprecipitating clouds on the
1063 aerosol size distribution in the marine boundary layer, Geophys. Res. Lett., 13(1),
1064 125–128, doi:10.1029/GL013i002p00125, 1987.

1065 Hu, Q.-H., Xie, Z.-Q., Wang, X.-M., Kang, H., He, Q.-F. and Zhang, P.: Secondary organic
1066 aerosols over oceans via oxidation of isoprene and monoterpenes from Arctic to
1067 Antarctic, Sci. Rep., 3, 2280, doi:10.1038/srep02280, 2013.

1068 Huntrieser, H., Heland, J., Schlager, H., Forster, C., Stohl, A., Aufmhoff, H., Arnold, F., Scheel,
1069 H. E., Campana, M., Gilge, S., Eixmann, R. and Cooper, O.: Intercontinental air
1070 pollution transport from North America to Europe : Experimental evidence from
1071 airborne measurements and surface observations, J. Geophys. Res., 110, D01305,
1072 doi:10.1029/2004JD005045, 2005.

1073 Iacono, M. J., Delamere, J. S., Mlawer, E. J., Shephard, M. W., Clough, S. A. and Collins, W. D.:
1074 Radiative forcing by long-lived greenhouse gases: Calculations with the AER
1075 radiative transfer models, J. Geophys. Res. Atmos., 113(13), D13103,
1076 doi:10.1029/2008JD009944, 2008.

1077 IPCC, 2013: *Climate Change 2013: The Physical Science Basis. Contribution of Working Group*
1078 *I to the Fifth Assessment Report of the Intergovernmental Panel on Climate*
1079 *Change* [Stocker, T.F., D. Qin, G.-K. Plattner, M. Tignor, S.K. Allen, J.
1080 Boschung, A. Nauels, Y. Xia, V. Bex and P.M. Midgley (eds.)]. Cambridge

University Press, Cambridge, United Kingdom and New York, NY, USA, 1535 pp.

Irish, V. E., Elizondo, P., Chen, J., Chou, C., Charette, J., Lizotte, M., Ladino, L. A., Wilson, T. W., Gosselin, M., Murray, B. J., Polishchuk, E., Abbatt, J. P. D., Miller, L. A., and Bertram, A. K.: Ice-nucleating particles in Canadian Arctic sea-surface microlayer and bulk seawater, Atmos. Chem. Phys., 17, 10583–10595, https://doi.org/10.5194/acp-17-10583-2017, 2017.

Jaeglé, L., Quinn, P. K., Bates, T. S., Alexander, B. and Lin, J. T.: Global distribution of sea salt aerosols: New constraints from in situ and remote sensing observations, Atmos. Chem. Phys., 11(7), 3137–3157, doi:10.5194/acp-11-3137-2011, 2011.

Jin, Q., Grandey, B. S., Rothenberg, D., Avramov, A. and Wang, C.: Impacts on cloud radiative effects induced by coexisting aerosols converted from international shipping and maritime DMS emissions, Atmos. Chem. Phys., 18, 16793–16808, https://doi.org/10.5194/acp-18-16793-2018, 2018.

Johnson, M. T.: A numerical scheme to calculate temperature and salinity dependent air-water transfer velocities for any gas, Ocean Sci., 6(4), 913–932, doi:10.5194/os-6-913-2010, 2010.

Karl, M., Leck, C., Gross, A. and Pirjola, L.: A study of new particle formation in the marine boundary layer over the central Arctic Ocean using a flexible multicomponent aerosol dynamic model, Tellus, Ser. B Chem. Phys. Meteorol., 64(1), 1–24, doi:10.3402/tellusb.v64i0.17158, 2012.

Kasparian, J., Hassler, C., Ibelings, B., Berti, N., Bigorre, S., Djambazova, V., Gascon-diez, E., Giuliani, G., Houlmann, R., Kiselev, D., Laborie, P. De, Le, A., Magouroux, T., Neri, T., Palomino, D., Pfändler, S., Ray, N., Sousa, G., Staedler, D., Tettamanti, F., Wolf, J. and Beniston, M.: Assessing the Dynamics of Organic Aerosols over the North Atlantic Ocean, Sci. Rep., 7, 45476, doi:10.1038/srep45476, 2017.

Kazil, J., Wang, H., Feingold, G., Clarke, A. D., Snider, J. R. and Bandy, A. R.: and Physics Modeling chemical and aerosol processes in the transition from closed to open cells during VOCALS-REx, Atmos. Chem. Phys., 11, 7491–7514, doi:10.5194/acp-11-7491-2011, 2011.

Kerminen, V. M., Anttila, T., Lehtinen, K. E. J. and Kulmala, M.: Parameterization for atmospheric new-particle formation: Application to a system involving sulfuric

acid and condensable water-soluble organic vapors, Aerosol Sci. Technol., 38(10), 1001–1008, doi:10.1080/027868290519085, 2004.

Kim, M. J., Novak, G. A., Zoerb, M. C., Yang, M., Blomquist, B. W., Huebert, B. J., Cappa, C. D. and Bertram, T. H.: Air-Sea exchange of biogenic volatile organic compounds and the impact on aerosol particle size distributions, Geophys. Res. Lett., 44(8), 3887–3896, doi:10.1002/2017GL072975, 2017.

Kodros, J. K., Cucinotta, R., Ridley, D. A., Wiedinmyer, C. and Pierce, J. R.: The aerosol radiative effects of uncontrolled combustion of domestic waste, Atmos. Chem. Phys., 16(11), 6771–6784, doi:10.5194/acp-16-6771-2016, 2016.

Kodros, J. K. and Pierce, J. R.: Important global and regional differences in aerosol cloud-albedo effect estimates between simulations with and without prognostic aerosol microphysics, J. Geophys. Res., 122(7), 4003–4018, doi:10.1002/2016JD025886, 2017.

Korhonen, H., Carslaw, K. S., Spracklen, D. V, Mann, G. W. and Woodhouse, M. T.: Influence of oceanic dimethyl sulfide emissions on cloud condensation nuclei concentrations and seasonality over the remote Southern Hemisphere oceans: A global model study, J. Geophys. Res. Atmos., 113(D15), doi:10.1029/2007JD009718, 2008

Kuang, C., Senum, G. I., Dedrick, J., Leaitch, W. R., Lubin, D., Aiken, A. C., Springston, S. R., Uin, J., Russell, L. M. and Liu, J.: High summertime aerosol organic functional group concentrations from marine and seabird sources at Ross Island, Antarctica, during AWARE, Atmos. Chem. Phys., 18(12), 8571–8587, doi:10.5194/acp-18-8571-2018, 2018.

Kulmala, M., Lehtinen, K. E. J., and Laaksonen, A.: Cluster activation theory as an explanation of the linear dependence between formation rate of 3nm particles and sulphuric acid concentration, Atmos. Chem. Phys., 6, 787–793, https://doi.org/10.5194/acp-6-787-2006, 2006.

Lana, A., Bell, T. G., Simó, R., Vallina, S. M., Ballabrera-Poy, J., Kettle, A. J., Dachs, J., Bopp, L., Saltzman, E. S., Stefels, J., Johnson, J. E. and Liss, P. S.: An updated climatology of surface dimethlysulfide concentrations and emission fluxes in the global ocean, Global Biogeochem. Cycles, 25(1), 1–17, doi:10.1029/2010GB003850, 2011.

1144 Lana, A., Simó, R., Vallina, S. M. and Dachs, J.: Re-examination of global emerging patterns of
1145      ocean DMS concentration, Biogeochemistry, 110(1), 173–182,
1146      doi:10.1007/s10533-011-9677-9, 2012a.

1147 Lana, A., Simó, R., Vallina, S. M., and Dachs, J.: Potential for a biogenic influence on cloud
1148      microphysics over the ocean: a correlation study with satellite-derived data, Atmos.
1149      Chem. Phys., 12, 7977–7993, https://doi.org/10.5194/acp-12-7977-2012, 2012b.

1150 Leaitch, W. R., Sharma, S., Huang, L., Toom-Sauntry, D., Chivulescu, A., Macdonald, A. M., von
1151      Salzen, K., Pierce, J. R., Bertram, A. K., Schroder, J. C., Shantz, N. C., Chang, R.
1152      Y.-W. and Norman, A.-L.: Dimethyl sulfide control of the clean summertime Arctic
1153      aerosol and cloud, Elem. Sci. Anthr., 1, 000017,
1154      doi:10.12952/journal.elementa.000017, 2013.

1155 Leaitch, R. W., Russell, L. M., Liu, J., Kolonjari, F., Toom, D., Huang, L., Sharma, S., Chivulescu,
1156      A., Veber, D. and Zhang, W.: Organic functional groups in the submicron aerosol
1157      at 82.5 degrees N, 62.5 degrees W from 2012 to 2014, Atmos. Chem. Phys., 18,
1158      3269–3287, doi:10.5194/acp-18-3269-2018, 2018.

1159 Leck, C. and Bigg, E. K.: Source and evolution of the marine aerosol—A new perspective,
1160      Geophys. Res. Lett., 32(19), doi:10.1029/2005GL023651, 2005.

1161 Lee, Y. H. and Adams, P. J.: A fast and efficient version of the TwO-Moment Aerosol Sectional
1162      (TOMAS) global aerosol microphysics model, Aerosol Sci. Technol., 46(6), 678–
1163      689, doi:10.1080/02786826.2011.643259, 2012.

1164 Lee, Y. H., Pierce, J. R., and Adams, P. J.: Representation of nucleation mode microphysics in a
1165      global aerosol model with sectional microphysics, Geosci. Model Dev., 6, 1221–
1166      1232, https://doi.org/10.5194/gmd-6-1221-2013, 2013.

1167 Liu, H., Jacob, D. J., Bey, I. and Yantosca, R. M.: Constraints from210Pb and7Be on wet
1168      deposition and transport in a global three-dimensional chemical tracer model driven
1169      by assimilated meteorological fields, J. Geophys. Res. Atmos., 106(D11), 12109–
1170      12128, doi:10.1029/2000JD900839, 2001.

1171 Lohmann, U. and Feichter, J.: Global indirect aerosol effects: a review, Atmos. Chem. Phys., 5(3),
1172      715–737, doi:10.5194/acp-5-715-2005, 2005.

1173 Luo, G., Yu, F. and Schwab, J.: Revised treatment of wet scavenging processes dramatically
1174      improves GEOS-Chem 12 . 0 . 0 simulations of surface nitric acid, nitrate, and

1175   ammonium over the United States, Geosci. Model. Dev., 12, 3439–3447,
1176   doi.10.5194/gmd-12-3439-2019, 2019.

1177 Luo, G., Yu, F. and Moch, J. M.: Further improvement of wet process treatments in GEOS-Chem
1178   v12 . 6 . 0 : impact on global distributions of aerosols and aerosol precursors,
1179   Geosci. Model Dev., 2879–2903, 2020.

1180 Mahmood, R., Salzen, K. Von, Norman, A., Galí, M. and Levasseur, M.: Sensitivity of Arctic
1181   sulfate aerosol and clouds to changes in future surface seawater dimethylsulfide
1182   concentrations, Atmos. Chem. Phys., 19, 6419–6435, https://doi.org/10.5194/acp-
1183   19-6419-2019, 2019.

1184 Mårtensson, E. M., Nilsson, E. D., de Leeuw, G., Cohen, L. H. and Hansson, H.-C.: Laboratory
1185   simulations and parameterization of the primary marine aerosol production, J.
1186   Geophys. Res. Atmos., 108(D9), n/a-n/a, doi:10.1029/2002JD002263, 2003.

1187 McCoy, D. T., Burrows, S. M., Wood, R., Grosvenor, D. P., Elliott, S. M., Ma, P.-L., Rasch, P. J.
1188   and Hartmann, D. L.: Natural aerosols explain seasonal and spatial patterns of
1189   Southern Ocean cloud albedo, Sci. Adv., 1(6), e1500157,
1190   doi:10.1126/sciadv.1500157, 2015.

1191 McDuffie, E. E., Smith, S. J., O'Rourke, P., Tibrewal, K., Venkataraman, C., Marais, E. A., Zheng,
1192   B., Crippa, M., Brauer, M., and Martin, R. V.: A global anthropogenic emission
1193   inventory of atmospheric pollutants from sector- and fuel-specific sources (1970–
1194   2017): An application of the Community Emissions Data System (CEDS), Earth
1195   Syst. Sci. Data Discuss., https://doi.org/10.5194/essd-2020-103, in review, 2020.

1196 McNaughton, C. S., Clarke, A. D., Howell, S. G., Pinkerton, M., Anderson, B., Thornhill, L.,
1197   Hudgins, C., et al.: Results from the DC-8 Inlet Characterization Experiment
1198   (DICE): Airborne versus surface sampling of mineral dust and sea salt aerosols,
1199   Aerosol Sci. Tech. 41, (2). 136-159, 2007.

1200 Meskhidze, N., Sabolis, A., Reed, R. and Kamykowski, D.: Quantifying environmental stress-
1201   induced emissions of algal isoprene and monoterpenes using laboratory
1202   measurements, Biogeosciences, 12, 637–651, doi:10.5194/bg-12-637-2015, 2015.

1203 Monahan, E. C., Fairall, C. W., Davidson, K. L., and Boyle, P. J.: Observed inter-relations between
1204   10m winds, ocean whitecaps and marine aerosols, Q. J. Roy. Meteor. Soc., 109,
1205   379–392, 1983.

Müller, M., Mikoviny, T., Feil, S., Haidacher, S., Hanel, G., Hartungen, E., Jordan, A., Märk, L., Mutschlechner, P., Schottkowsky, R., Sulzer, P., Crawford, J. H., and Wisthaler, A.: A compact PTR-ToF-MS instrument for airborne measurements of VOCs at high spatio-temporal resolution, Atmos. Meas. Tech. 7, 3763-3772, doi:10.5194/amt-7-3763-2014, 2014.

Mungall, E. L., Abbatt, J. P. D., Wentzell, J. J. B., Lee, A. K. Y., Thomas, J. L., Blais, M., Gosselin, M., Miller, L. A., Papakyriakou, T., Willis, M. D. and Liggio, J.: Microlayer source of oxygenated volatile organic compounds in the summertime marine Arctic boundary layer, Proc. Natl. Acad. Sci., 114(24), 6203–6208, doi:10.1073/pnas.1620571114, 2017.

Napari, I., Noppel, M., Vehkamaki, H. and Kulmala, M.: Parametrization of ternary nucleation rates for H2SO4-NH3-H2O vapors, J. Geophys. Res. Atmos., 107(19), 2–7, doi:10.1029/2002JD002132, 2002.

Nightingale, P. D., Liss, P. S. and Schlosser, P.: Measurements of air-sea gas transfer during an open ocean algal bloom, Geophys. Res. Lett., 27(14), 2117–2120, doi:10.1029/2000GL011541, 2000a.

Nightingale, P. D., Malin, G., Law, C. S., Watson, A. J., Liss, P. S., Liddicoat, M. I., Boutin, J. and Upstill-Goddard, R. C.: In situ evaluation of air-sea gas exchange parameterizations using novel conservative and volatile tracers, Global Biogeochem. Cycles, 14(1), 373–387, doi:10.1029/1999GB900091, 2000b.

O'Dowd, C. D., Smith, M. H., Consterdine, I. E., Lowe, J. A.: Marine aerosol, sea-salt, and the marine sulphur cycle: A short review. Atmos. Environ. 31, 73–80 (1997)

O'Dowd, C. D.: Marine aerosol formation from biogenic iodine emissions, Nature, 417(June), 1–5, doi:10.1038/nature00775, 2002.

O' Dowd, C. D., Facchini, M. C., Cavalli, F., Ceburnis, D., Mircea, M., Decesari, S., Fuzzi, S., Yoon, Y. J. and Putaud, J.: Biogenically driven organic contribution to marine aerosol, Nature, 431(7009), 676-680, https://doi.org/10.1038/nature02959, 2004

O'Dowd, C. D. and de Leeuw, G.: Marine aerosol production : a review of the current knowledge, Phil. Trans. R. Soc. A, 1(May), 1753–1774, doi:10.1098/rsta.2007.2043, 2007.

O'Dowd, C. D., Ceburnis, D., Ovadnevaite, J., Bialek, J., Stengel, D. B., Zacharias, M., Nitschke, U., Connan, S., Rinaldi, M., Fuzzi, S., Decesari, S., Facchini, M. C., Marullo, S.,

1261   Santoleri, R., Anno, A. D., Corinaldesi, C., Tangherlini, M. and Danovaro, R.:
1262   Connecting marine productivity to sea-spray via nanoscale biological processes :
1263   Phytoplankton Dance or Death Disco?, Sci. Rep, 5(May), 14883, 1–11,
1264   doi:10.1038/srep14883, 2015.

1265 Ovadnevaite, J., Ceburnis, D., Martucci, G., Bialek, J., Monahan, C., Rinaldi, M., Facchini, M. C.,
1266   Berresheim, H., Worsnop, D. R. and O'Dowd, C.: Primary marine organic aerosol :
1267   A dichotomy of low hygroscopicity and high CCN activity, Geophys. Res. Lett.,
1268   38, L21806 1–5, doi:10.1029/2011GL048869, 2011.

1269 Ovadnevaite, J., Ceburnis, D., Canagaratna, M., Berresheim, H., Bialek, J., Martucci, G., Worsnop,
1270   D. R. and Dowd, C. O.: On the effect of wind speed on submicron sea salt mass
1271   concentrations and source fluxes, J. Geophys. Res.,, 117, D16201, 1–11,
1272   doi:10.1029/2011JD017379, 2012.

1273 Pai, S. J., Heald, C. L., Pierce, J. R., Farina, S. C., Marais, E. A., Jimenez, J. L., Campuzano-jost,
1274   P., Nault, B. A., Middlebrook, A. M., Coe, H., Shilling, J. E., Bahreini, R., Dingle,
1275   J. H. and Vu, K.: An evaluation of global organic aerosol schemes using airborne
1276   observations, Atmos. Chem. Phys., 20 , 2637–2665, https://doi.org/10.5194/acp-
1277   20-2637-2020, 2020.

1278 Park, K.-T., Jang, S., Lee, K., Yoon, Y. J., Kim, M.-S., Park, K., Cho, H.-J., Kang, J.-H., Udisti,
1279   R., Lee, B.-Y. and Shin, K.-H.: Observational evidence for the formation of DMS-
1280   derived aerosols during Arctic phytoplankton blooms, Atmos. Chem. Phys., 17(15),
1281   9665–9675, doi:https://doi.org/10.5194/acp-17-9665-2017, 2017.

1282 Park, K.-T., Lee, K., Kim, T.-W., Yoon, Y. J., Jang, E.-H., Jang, S., Lee, B.-Y. and Hermansen,
1283   O.: Atmospheric DMS in the Arctic Ocean and Its Relation to Phytoplankton
1284   Biomass, Global Biogeochem. Cycles, 32(3), 351–359,
1285   doi:10.1002/2017GB005805, 2018.

1286 Pierce, J. R., Croft, B., Kodros, J. K., D'Andrea, S. D. and Martin, R. V.: The importance of
1287   interstitial particle scavenging by cloud droplets in shaping the remote aerosol size
1288   distribution and global aerosol-climate effects, Atmos. Chem. Phys., 15(11), 6147–
1289   6158, doi:10.5194/acp-15-6147-2015, 2015.

1290 Prather, K. A., Bertram, T. H., Grassian, V. H., Deane, G. B., Stokes, M. D., DeMott, P. J.,
1291   Aluwihare, L. I., Palenik, B. P., Azam, F., Seinfeld, J. H., Moffet, R. C., Molina,

1292   M. J., Cappa, C. D., Geiger, F. M., Roberts, G. C., Russell, L. M., Ault, A. P.,
1293   Baltrusaitis, J., Collins, D. B., Corrigan, C. E., Cuadra-Rodriguez, L. A., Ebben, C.
1294   J., Forestieri, S. D., Guasco, T. L., Hersey, S. P., Kim, M. J., Lambert, W. F.,
1295   Modini, R. L., Mui, W., Pedler, B. E., Ruppel, M. J., Ryder, O. S., Schoepp, N. G.,
1296   Sullivan, R. C. and Zhao, D.: Bringing the ocean into the laboratory to probe the
1297   chemical complexity of sea spray aerosol, Proc. Natl. Acad. Sci., 110(19), 7550–
1298   7555, doi:10.1073/pnas.1300262110, 2013.

1299   Quinn, P. K. and Bates, T. S.: The case against climate regulation via oceanic phytoplankton
1300   sulphur emissions, Nature, 480(7375), 51–56, doi:10.1038/nature10580, 2011.

1301   Quinn, P. K., Bates, T. S., Schulz, K. S., Coffman, D. J., Frossard, A. A., Russell, L. M., Keene,
1302   W. C. and Kieber, D. J.: Contribution of sea surface carbon pool to organic matter
1303   enrichment   in   sea   spray   aerosol,   Nat.   Geosci.,   7(3),   228–232,
1304   doi:10.1038/ngeo2092, 2014.

1305   Quinn, P. K., Collins, D. B., Grassian, V. H., Prather, K. A. and Bates, T. S.: Chemistry and Related
1306   Properties of Freshly Emitted Sea Spray Aerosol, Chem. Rev., 115(10), 4383–
1307   4399, doi:10.1021/cr500713g, 2015.

1308   Quinn, P. K., Coffman, D. J., Johnson, J. E., Upchurch, L. M. and Bates, T. S.: Small fraction of
1309   marine cloud condensation nuclei made up of sea spray aerosol, Nat. Geosci., 10(9),
1310   674–679, doi:10.1038/ngeo3003, 2017.

1311   Quinn, P. K., Bates, T. S., Coffman, D. J., Upchurch, L., Johnson, J. E., Moore, R. and Ziemba,
1312   L.: Seasonal Variations in Western North Atlantic Remote Marine Aerosol
1313   Properties,   J.   Geophys.   Res.,   Atmos.,   124,   14,240–14,261.
1314   https://doi.org/10.1029/2019JD031740, 2019.

1315   Park, K.-T., Lee, K., Kim, T.-W., Yoon, Y. J., Jang, E.-H., Jang, S., Lee, B.-Y. and Hermansen,
1316   O.: Atmospheric DMS in the Arctic Ocean and Its Relation to Phytoplankton
1317   Biomass, Global Biogeochem. Cycles, 32(3), 351–359,
1318   doi:10.1002/2017GB005805, 2018.

1319   Ramnarine, E., Kodros, J. K., Hodshire, A. L., Lonsdale, C. R., Alvarado, M. J. and Pierce, J. R.:
1320   Effects of near-source coagulation of biomass burning aerosols on global
1321   predictions of aerosol size distributions and implications for aerosol radiative

1322   effects, Atmos. Chem. Phys., 19, 6561–6577, https://doi.org/10.5194/acp-19-
1323   6561-2019, 2019.

1324   Rempillo, O., Seguin, A. M., Norman, A.-L., Scarratt, M., Michaud, S., Chang, R., Sjostedt, S.,
1325   Abbatt, J., Else, B., Papakyriakou, T., Sharma, S., Grasby, S. and Levasseur, M.:
1326   Dimethyl sulfide air-sea fluxes and biogenic sulfur as a source of new aerosols in
1327   the Arctic fall, J. Geophys. Res. Atmos., 116, (D100S04),
1328   doi:10.1029/2011JD016336, 2011.

1329   Revell, L. E., Kremser, S., Hartery, S., Harvey, M., Mulcahy, J. P., Williams, J., Morgenstern, O.,
1330   Mcdonald, A. J., Varma, V., Bird, L. and Schuddeboom, A.: The sensitivity of
1331   Southern Ocean aerosols and cloud microphysics to sea spray and sulfate aerosol
1332   production in the HadGEM3-GA7 . 1 chemistry – climate model, Atmos. Chem.
1333   Phys., 19, 15447–15466, https://doi.org/10.5194/acp-19-15447-2019, 2019.

1334   Riccobono, F., Schobesberger, S., Scott, C. E., Dommen, J., Ortega, I. K., Rondo, L., Almeida, J.,
1335   Amorim, A., Bianchi, F., Breitenlechner, M., David, A., Downard, A., Dunne, E.
1336   M., Duplissy, J., Ehrhart, S., Flagan, R. C., Franchin, A., Hansel, A., Junninen, H.,
1337   Kajos, M., Keskinen, H., Kupc, A., Kupiainen, O., Kürten, A., Kurtén, T., Kvashin,
1338   A. N., Laaksonen, A., Lehtipalo, K., Makhmutov, V., Mathot, S., Nieminen, T.,
1339   Olenius, T., Onnela, A., Petäjä, T., Praplan, A. P., Santos, F. D., Schallhart, S.,
1340   Seinfeld, J. H., Sipilä, M., Spracklen, D. V, Stozhkov, Y., Stratmann, F., Tomé, A.,
1341   Tsagkogeorgas, G., Vaattovaara, P., Vehkamäki, H., Viisanen, Y., Vrtala, A.,
1342   Wagner, P. E., Weingartner, E., Wex, H., Wimmer, D., Carslaw, K. S., Curtius, J.,
1343   Donahue, N. M., Kirkby, J., Kulmala, M., Worsnop, D. R., Baltensperger, U. U. .,
1344   Schobesberger, S., Scott, C. E., Dommen, J., Ortega, I. K., Rondo, L., Almeida, J.,
1345   Amorim, A., Bianchi, F., Breitenlechner, M., David, A., Downard, A., Dunne, E.
1346   M., Duplissy, J., Ehrhart, S., Flagan, R. C., Franchin, A., Hansel, A., Junninen, H.,
1347   Kajos, M., Keskinen, H., Kupc, A., Kürten, A., Kvashin, A. N., Laaksonen, A.,
1348   Lehtipalo, K., Makhmutov, V., Mathot, S., Nieminen, T., Onnela, A., Petäjä, T.,
1349   Praplan, A. P., Santos, F. D., Schallhart, S., Seinfeld, J. H., Sipilä, M., Spracklen,
1350   D. V, Stozhkov, Y., Stratmann, F., Tomé, A., Tsagkogeorgas, G., et al.: Oxidation
1351   Products of Biogenic Emissions Contribute to Nucleation of Atmospheric Particles,
1352   Science, 344(May), 717–721 [online] Available from:

http://www.sciencemag.org/content/344/6185/717.abstract, doi: 10.1126/science.1243527, 2014.

Rinaldi, M., Decesari, S., Finessi, E., Giulianelli, L., Carbone, C., Fuzzi, S., O'Dowd, C., Ceburnis, D. and Facchini, M. C.: Primary and Secondary Organic Marine Aerosol and Oceanic Biological Activity: Recent Results and New Perspectives for Future Studies, Adv. Meteorol., 2010, 1–10, doi:10.1155/2010/310682, 2010.

Rodríguez-Ros, P., Cortés, P., Robinson, C. M., Nunes, S., Hassler, C., Royer, S., Estrada, M. and Simó, R.: Distribution and Drivers of Marine Isoprene Concentration across the Southern Ocean, Atmosphere, 11, 556, 1–19, doi:10.3390/atmos11060556, 2020a.

Rodriguez-Ros, P., Galí, M., Cortés, P., Robinson, C. M., Antoine, D., Wohl, C., Yang, M. and Simó, R.: Remote Sensing Retrieval of Isoprene Concentrations in the Southern Ocean Geophys. Res. Lett., 47, e2020GL087888, 1–10, doi:10.1029/2020GL087888, 2020b.

Russell, L. M., Hawkins, L. N., Frossard, A. A., Quinn, P. K. and Bates, T. S.: Carbohydrate-like composition of submicron atmospheric particles and their production from ocean bubble bursting, Proc. Natl. Acad. Sci., 107(15), 6652-6657, doi:10.1073/pnas.0908905107, 2010.

Saliba, G., Chen, C., Lewis, S., Russell, L. M., Rivellini, L., Lee, A. K. Y., Carlson, C. A. and Behrenfeld, M. J.: Factors driving the seasonal and hourly variability of sea-spray aerosol number in the North Atlantic, Proc, Nat. Acad. Sci., 116(41), 20309–20314, doi:10.1073/pnas.1907574116, 2019.

Saliba, G., Chen, C., Lewis, S., Russell, L. M., Quinn, P. K., Bates, T. S., Bell, T. G., Lawler, M. J., Saltzman, E. S., Sanchez, K. J., Moore, R., Shook, M., Rivellini, L., Lee, A.K. Y. Baetge, N., , Carlson, C. A. and Behrenfeld, M. J.L Seasonal differences and variability of concentrations, chemical composition, and cloud condensation nuclei of marine aerosol over the North Atlantic, submitted (2020).

Sanchez, K. J., Chen, C.-L., Russell, L. M., Betha, R., Liu, J., Price, D. J., Massoli, P., Ziemba, L. D., Crosbie, E. C., Moore, R. H., Müller, M., Schiller, S. A., Wisthaler, A., Lee, A. K. Y., Quinn, P. K., Bates, T. S., Porter, J., Bell, T. G., Saltzman, E. S., Vaillancourt, R. D. and Behrenfeld, M. J.: Substantial Seasonal Contribution of Observed Biogenic Sulfate Particles to Cloud Condensation Nuclei, Sci. Rep., 8(1),

1384   3235, doi:10.1038/s41598-018-21590-9, 2018.

1385   Savoie, D. L., R. Arimoto, W. C. Keene, J. M. Prospero, R. A. Duce, and J. N. Galloway, Marine
1386   biogenic and anthropogenic contributions to non-sea-salt sulfate in the marine
1387   boundary layer over the North Atlantic Ocean, J. Geophys. Res., 107(D18), 4356,
1388   doi:10.1029/2001JD000970, 2002

1389   Schwarz, J. P., Gao, R. S., Fahey, D. W., Thomson, D. S., Watts, L. A., Wilson, J. C., Reeves, J.
1390   M., Darbeheshti, M., Baumgardner, D. G., Kok, G. L., Chung, S. H., Schulz, M.,
1391   Hendricks, J., Lauer, A., Ka, B. and Slowik, J. G.: Single-particle measurements of
1392   midlatitude black carbon and light-scattering aerosols from the boundary layer to
1393   the lower stratosphere, J. Geophys. Res. Atmos., 111, D216207, 1–15,
1394   doi:10.1029/2006JD007076, 2006.

1395   Schiffer, J. M., Mael, L. E., Prather, K. A., Amaro, R. E. and Grassian, V. H.: Sea Spray Aerosol:
1396   Where Marine Biology Meets Atmospheric Chemistry, ACS Cent. Sci., 4, 1617-
1397   1623 doi:10.1021/acscentsci.8b00674, 2018.

1398   Schiller, S. A. P.: Flugzeuggestützte Messung flüchtiger organischer Verbindungen über dem
1399   Nordatlantik mittels PTR-ToF-MS, Master Thesis (*in German*), Universität
1400   Innsbruck (2018)

1401   Schwinger, J., Tjiputra, J., Goris, N., Six, K. D., Kirkevåg, A., Seland, Ø., Heinze, C. and Ilyina,
1402   T.: Amplification of global warming through pH dependence of DMS production
1403   simulated with a fully coupled Earth system model, Biogeosciences, 14, 3633–
1404   3648, https://doi.org/10.5194/bg-14-3633-2017, 2017.

1405   Sharma, S., Lavoué, D., Cachier, H., Barrie, L. A. and Gong, S. L.: Long-term trends of the black
1406   carbon concentrations in the Canadian Arctic, J. Geophys. Res. Atmos., 109,
1407   (D15203), doi:10.1029/2003JD004331, 2004.

1408   Sharma, S., Andrews, E., Barrie, L. A., Ogren, J. A. and Lavoué, D.: Variations and sources of the
1409   equivalent black carbon in the high Arctic revealed by long-term observations at
1410   Alert and Barrow: 1989–2003, J. Geophys. Res. Atmos., 111, (D14208),
1411   doi:10.1029/2005JD006581, 2006.

1412   Sihto, S., Kulmala, M., Kerminen, V., Maso, M. D. and Petäjä, T., Riipinen, I., Korhonen, H.,
1413   Arnold, F., Janson, R., Boy, M., Laaksonen, A. and Lehtinen, K. E. J.: Atmospheric

sulphuric acid and aerosol formation : implications from atmospheric
measurements for nucleation and early growth mechanisms, Atmos. Chem. Phys.,
6, 4079–4091, www.atmos-chem-phys.net/6/4079/2006/, 2006.

Singh, H. B., Cai, C., Kaduwela, A., Weinheimer, A. and Wisthaler, A.: Interactions of fire
emissions and urban pollution over California : Ozone formation and air quality
simulations, Atmos. Environ., 56, 45–51, doi:10.1016/j.atmosenv.2012.03.046,
2012.

Stohl, A., Forster, C., Eckhardt, S., Spichtinger, N., Huntrieser, H., Heland, J., Schlager, H.,
Wilhelm, S., Arnold, F. and Cooper, O.: A backward modeling study of
intercontinental pollution transport using aircraft measurements, J. Geophys. Res.,
108, D12, 4370, doi:10.1029/2002JD002862, 2003.

Takegawa, N., Seto, T., Moteki, N., Koike, M., Oshima, N., Adachi, K., Kita, K., Takami, A. and
Kondo, Y.: Enhanced New Particle Formation Above the Marine Boundary Layer
Over the Yellow Sea : Potential Impacts on Cloud Condensation Nuclei, J.
Geophys. Res. Atmos., 125, e2019JD031448, 1–17, doi:10.1029/2019JD031448,
2020.

Tremblay, S., Picard, J.-C, Bachelder, J. O., Lutsch, E., Strong, K., Fogal, P., Leaitch, W. R.,
Sharma, S., Kolonjari, F., Cox, C. J., Chang, R. Y.-W. and Hayes, P. L.:
Characterization of aerosol growth events over Ellesmere Island during summers
of 2015 and 2016, Atmos. Chem. Phys., 19, 5589-
5604, https://doi.org/10.5194/acp-19-5589-2019, 2019.

Tunved, P., Ström, J. and Krejci, R.: Arctic aerosol life cycle: Linking aerosol size distributions
observed between 2000 and 2010 with air mass transport and precipitation at
Zeppelin station, Ny-Ålesund, Svalbard, Atmos. Chem. Phys., 13(7), 3643–3660,
doi:10.5194/acp-13-3643-2013, 2013.

van der Werf, G. R., Randerson, J. T., Giglio, L., Van Leeuwen, T. T., Chen, Y., Rogers, B. M.,
Mu, M., Van Marle, M. J. E., Morton, D. C., Collatz, G. J., Yokelson, R. J. and
Kasibhatla, P. S.: Global fire emissions estimates during 1997-2016, Earth Syst.
Sci. Data, 9(2), 697–720, doi:10.5194/essd-9-697-2017, 2017.

Vehkamäki, H., Kulmala, M., Napari, I., Lehtinen, K. E. J., Timmreck, C., Noppel, M. and
Laaksonen, A.: An improved parameterization for sulfuric acid – water nucleation

1445   rates for tropospheric and stratospheric conditions, J. Geophys. Res., 107, D22,
1446   4622, 1–10, doi:10.1029/2002JD002184, 2002.

1447 Veres, P. R., Neuman, J. A., Bertram, T. H., Assaf, E. and Wolfe, G. M.: Global airborne sampling
1448   reveals a previously unobserved dimethyl sulfide oxidation mechanism in the
1449   marine atmosphere, Proc.Natl, Acad. Sci., 117(9), 4505–4510,
1450   doi:10.1073/pnas.1919344117, 2020.

1451 Vinken, G. C. M., Boersma, K. F., Jacob, D. J., Meijer, E. W.: Accounting for non-linear chemistry
1452   of ship plumes in the GEOS-Chem global chemistry transport model, Atmos.
1453   Chem. Phys., 11, 11707–11722, doi:10.5194/acp-11-11707-2011, 2011.

1454 Wang, Q., Jacob, D. J., Fisher, J. A., Mao, J., Leibensperger, E. M., Carouge, C. C., Le Sager, P.,
1455   Kondo, Y., Jimenez, J. L., Cubison, M. J. and Doherty, S. J.: Sources of
1456   carbonaceous aerosols and deposited black carbon in the Arctic in winter-spring:
1457   Implications for radiative forcing, Atmos. Chem. Phys., 11, 12453–12473,
1458   doi:10.5194/acp-11-12453-2011, 2011.

1459 Wang, Q., Jacob, D. J., Spackman, J. R., Perring, A. E., Schwarz, J. P., Moteki, N., Marais, E. A.,
1460   Ge, C., Wang, J. and Barrett, S. R. H.: Global budget and radiative forcing of black
1461   carbon aerosol : Constraints from pole-to-pole (HIPPO) observations across the
1462   Pacific, J. Geophys. Res., 119, 195–206, doi:10.1002/2013JD020824, 2014.

1463 Wang, X., Sultana, C. M., Trueblood, J., Hill, T. C. J., Malfatti, F., Lee, C., Laskina, O., Moore,
1464   K. A., Beall, C. M., McCluskey, C. S., Cornwell, G. C., Zhou, Y., Cox, J. L.,
1465   Pendergraft, M. A., Santander, M. V., Bertram, T. H., Cappa, C. D., Azam, F.,
1466   DeMott, P. J., Grassian, V. H. and Prather, K. A.: Microbial control of sea spray
1467   aerosol composition: A tale of two blooms, ACS Cent. Sci., 1(3), 124–131,
1468   doi:10.1021/acscentsci.5b00148, 2015.

1469 Weber, R. J., Chen, G., Davis, D. D., Mauldin, R. L., Tanner, D. J., Clarke, A. D., Thornton, D.
1470   C. and Bandy, A. R.: Measurements of enhanced H_2SO_4 and 3-4 nm particles near
1471   a frontal cloud during the First Aerosol Characterization Experiment (ACE 1), J.
1472   Geophys. Res., 106, (D20),24 107 - 24117, 2001.

1473 Wehner, B., Werner, F., Ditas, F., Shaw, R. A., Kulmala, M. and Siebert, H.: Observations of new
1474   particle formation in enhanced UV irradiance zones near cumulus clouds, Atmos.
1475   Chem. Phys., 11701–11711, doi:10.5194/acp-15-11701-2015, 2015.

1476   Wesley, M. L.: Parameterization of surface resistances to gaseous deposition in regional-scale
1477   numerical models, Atmos. Environ., 23, 1293-1304, 1989.

1478   Westervelt, D. M.: Formation and growth of nucleated particles into cloud condensation nuclei :
1479   model – measurement comparison, Atmos. Chem. Phys., 13, 7645–7663,
1480   doi:10.5194/acp-13-7645-2013, 2013.

1481   Willis, M. D., Burkart, J., Thomas, J. L., Köllner, F., Schneider, J., Bozem, H., Hoor, P. M.,
1482   Aliabadi, A. A., Schulz, H., Herber, A. B., Leaitch, W. R. and Abbatt, J. P. D.:
1483   Growth of nucleation mode particles in the summertime Arctic: A case study,
1484   Atmos. Chem. Phys., 16(12), 7663–7679, doi:10.5194/acp-16-7663-2016, 2016.

1485   Willis, M. D., Köllner, F., Burkart, J., Bozem, H., Thomas, J. L., Schneider, J., Aliabadi, A. A.,
1486   Hoor, P. M., Schulz, H., Herber, A. B., Leaitch, W. R. and Abbatt, J. P. D.:
1487   Evidence for marine biogenic influence on summertime Arctic aerosol, Geophys.
1488   Res. Lett., 44(12), 6460–6470, doi:10.1002/2017GL073359, 2017.

1489   Willis, M. D., Leaitch, W. R. and Abbatt, J. P. D.: Processes Controlling the Composition and
1490   Abundance of Arctic Aerosol, Reviews of Geophysics, 56, 621-671,
1491   doi:10.1029/2018RG000602, 2018.

1492   Wood, R.: Stratocumulus Clouds, Mon. Weather Rev., 140, 2373–2423, doi:10.1175/MWR-D-11-
1493   00121.1, 2012.

1494   Wilson, T. W., Ladino, L. A., Alpert, P. A., Breckels, M. N., Brooks, I. M., Browse, J., Burrows,
1495   S. M., Carslaw, K. S., Huffman, J. A., Judd, C., Kilthau, W. P., Mason, R. H.,
1496   McFiggans, G., Miller, L. A., Najera, J. J., Polishchuk, E., Rae, S., Schiller, C. L.,
1497   Si, M., Temprado, J. V., Whale, T. F., Wong, J. P. S., Wurl, O., Yakobi-Hancock,
1498   J. D., Abbatt, J. P. D., Aller, J. Y., Bertram, A. K., Knopf, D. A. and Murray, B. J.:
1499   A marine biogenic source of atmospheric ice-nucleating particles, Nature,
1500   525(7568), 234–238, doi:10.1038/nature14986, 2015.

1501   Wood, R., Stemmler, J. D., Rémillard, J. and Jefferson, A.: Low-CCN concentration air masses
1502   over the eastern North Atlantic : Seasonality , meteorology , and drivers, J.
1503   Geophys. Res. Atmos., 122, 1203-1223, doi:10.1002/2016JD025557, 2017.

1504   Woodhouse, M. T., Mann, G. W., Carslaw, K. S. and Boucher, O.: Sensitivity of cloud
1505   condensation nuclei to regional changes in dimethyl-sulphide emissions, Atmos.
1506   Chem. Phys., 13(5), 2723–2733, doi:https://doi.org/10.5194/acp-13-2723-2013,

1507   2013.

1508 Xu, J. W., Martin, R. V., Morrow, A., Sharma, S., Huang, L., Richard Leaitch, W., Burkart, J.,
1509   Schulz, H., Zanatta, M., Willis, M. D., Henze, D. K., Lee, C. J., Herber, A. B. and
1510   Abbatt, J. P. D.: Source attribution of Arctic black carbon constrained by aircraft
1511   and surface measurements, Atmos. Chem. Phys., 17(19), 11971–11989,
1512   doi:10.5194/acp-17-11971-2017, 2017.

1513 Yassaa, N., Peeken, I., Zöllner, E., Bluhm, K., Arnold, S., Spracklan, D. and Williams, J: Evidence
1514   for marine production of monoterpenes, Environ. Chem., 5, 391–401,
1515   doi:10.1071/EN08047, 2008.

1516 Zanatta, M., Bozem, H., Köllner, F., Schneider, J., Hoor, P., Faria, J. De, Petzold, A., Bundke, U.,
1517   Staebler, R. M., Schulz, H., Herber, A. B., Zanatta, M., Bozem, H., Köllner, F.,
1518   Schneider, J., Hoor, P., Faria, J. De, Petzold, A., Bundke, U., Hayden, K., Staebler,
1519   R. M., Schulz, H. and Herber, A. B..: Airborne survey of trace gases amd aerosol
1520   over the Southern Baltic Sea: from clean marine boundary layer to shipping
1521   corridor effect, Tellus B Chem. Phys. Meteorol., 72(1), 1–24,
1522   doi:10.1080/16000889.2019.1695349, 2019.

1523 Zender, C. S., Bian, H. and Newman, D.: Mineral Dust Entrainment and Deposition (DEAD)
1524   model: Description and 1990s dust climatology, J. Geophys. Res., 108(D14), 4416,
1525   doi:10.1029/2002JD002775, 2003.

1526 Zhang, H. F., Worton, D. R., Lewandowski, M., Ortega, J., Rubitschun, C. L., Park, J. H.,
1527   Kristensen, K., Campuzano-Jost, P., Day, D. A., Jimenez, J. L., Jaoui, M.,
1528   Offenberg, J. H., Kleindienst, T. E., Gilman, J., Kuster, W. C., de Gouw, J., Park,
1529   C., Schade, G. W., Frossard, A. A., Russell, L., Kaser, L., Jud, W., Hansel, A.,
1530   Cappellin, L., Karl, T., Glasius, M., Guenther, A., Goldstein, A. H., Seinfeld, J. H.,
1531   Gold, A., Kamens, R. M. and Surratt, J. D.: Organosulfates as Tracers for
1532   Secondary Organic Aerosol (SOA) Formation from 2-Methyl-3-Buten-2-ol (MBO)
1533   in the Atmosphere, Environ. Sci. Technol., 46(17), 9437–9446,
1534   doi:10.1021/es301648z, 2012.

1535 Zheng, G., Wang, Y., Aiken, A. C., Gallo, F., Jensen, M. P., Kollias, P., Kuang, C., Luke, E.,
1536   Springston, S., Uin, J., Wood, R. and Wang, J.: Marine boundary layer aerosol in
1537   the eastern North Atlantic : seasonal variations and key controlling processes,

1538   Atmos. Chem. Phys., 18, 17615–17635, https://doi.org/10.5194/acp-18-17615-

1539   2018, 2018.

1540   Zheng, G., Kuang, C., Uin, J., Watson, T., and Wang, J.: Large contribution of organics to

1541   condensational growth and formation of cloud condensation nuclei (CCN) in

1542   remote marine boundary layer, Atmos. Chem. Phys. Discuss.,

1543   https://doi.org/10.5194/acp-2020-625, in review, 2020a.

1544   Zheng, G., Sedlacek, A. J., Aiken, A. C., Feng, Y., Watson, T. B., Raveh-rubin, S., Uin, J., Lewis,

1545   E. R. and Wang, J.: Long-range transported North American wild fire aerosols

1546   observed in marine boundary layer of eastern North Atlantic, Environ. Int.,

1547   139(March), 105680, doi:10.1016/j.envint.2020.105680, 2020b.

1548

1549

1550   **Figures and tables**
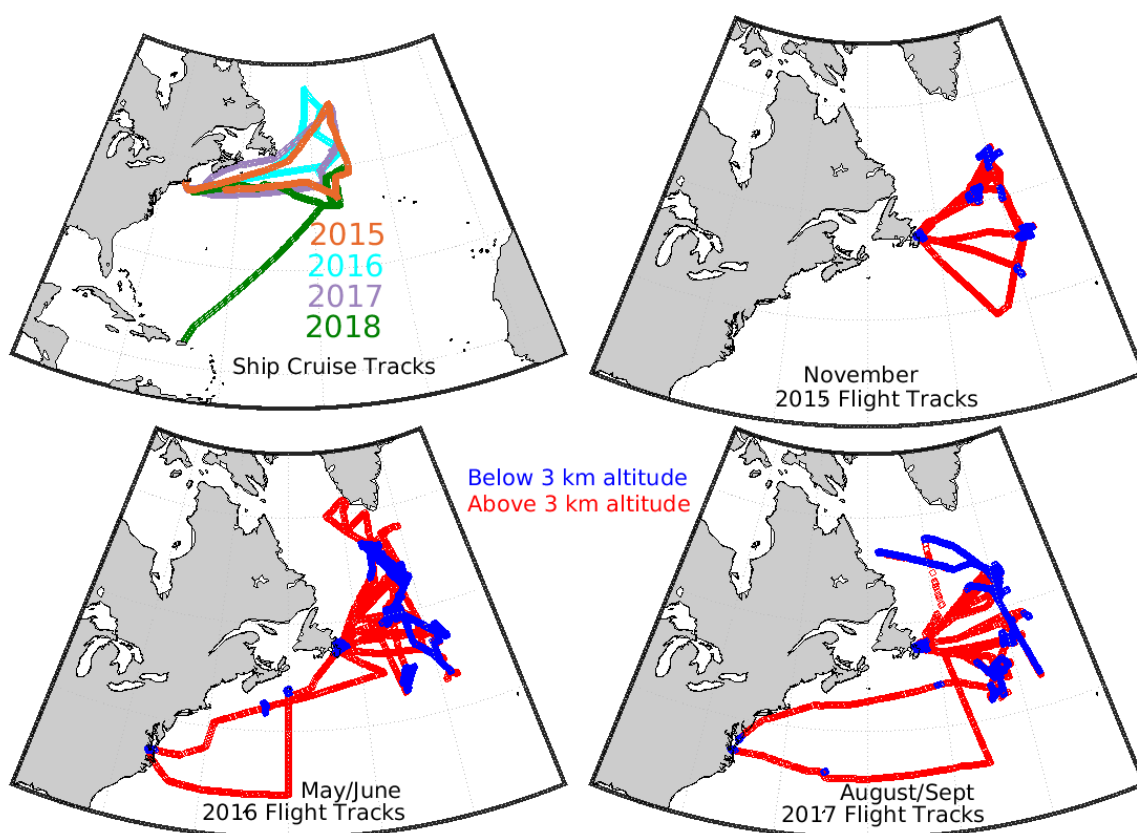
1551

1552 **Figure 1:** Cruise and aircraft tracks for the 2015-2018 NAAMES campaigns. Flight altitudes

1553 below 3 km are color-coded in medium blue and above 3 km in red. Ship tracks campaigns are

1554 color-coded for each year as shown by the legend, and as follows: Orange: November 2015

1555 winter transition (bloom minima); Cyan: May/June 2016 climax transition (bloom maxima);

1556 Purple: August/September 2017 declining phase; Green: March/April 2018 accumulation phase.

1557

1558

1559
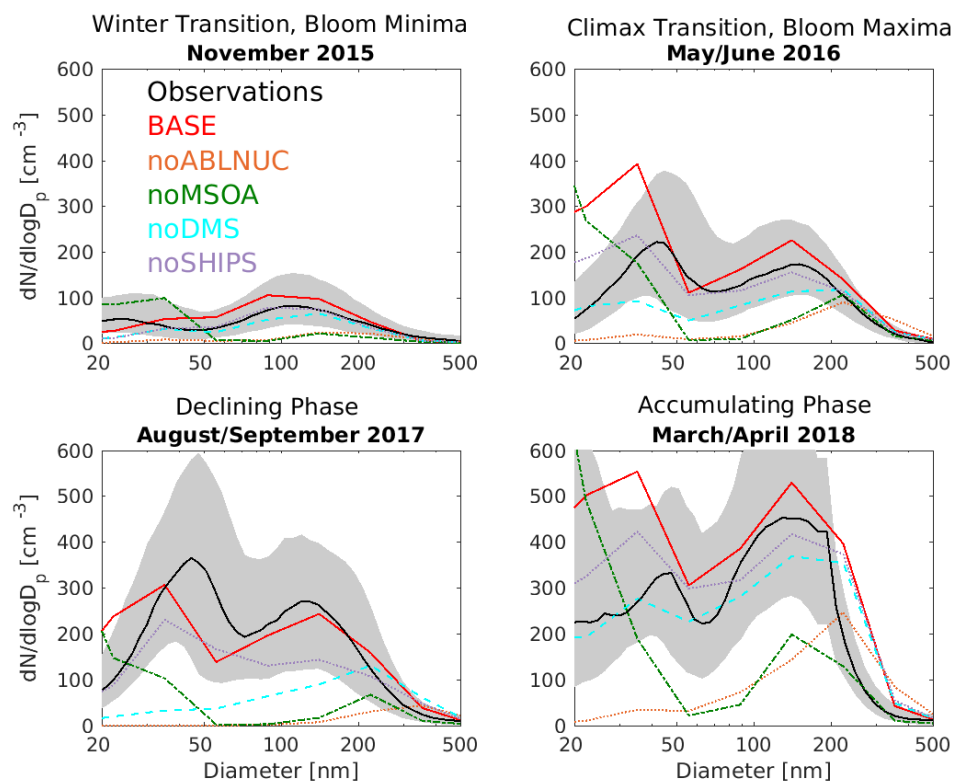
Figure 2: NAAMES cruise-track campaign-median marine boundary layer aerosol size distributions from marine-influenced SEMS observations (black, with 25th to 75th percentiles in grey) and for the five GEOS-Chem-TOMAS simulations as described in Table 1 (color-coded as shown in legend). Linestyles: Solid: Observations, BASE; Dotted: noABLNUC, noSHIPS; Dash-dot: noMSOA; Dashed: noDMS.
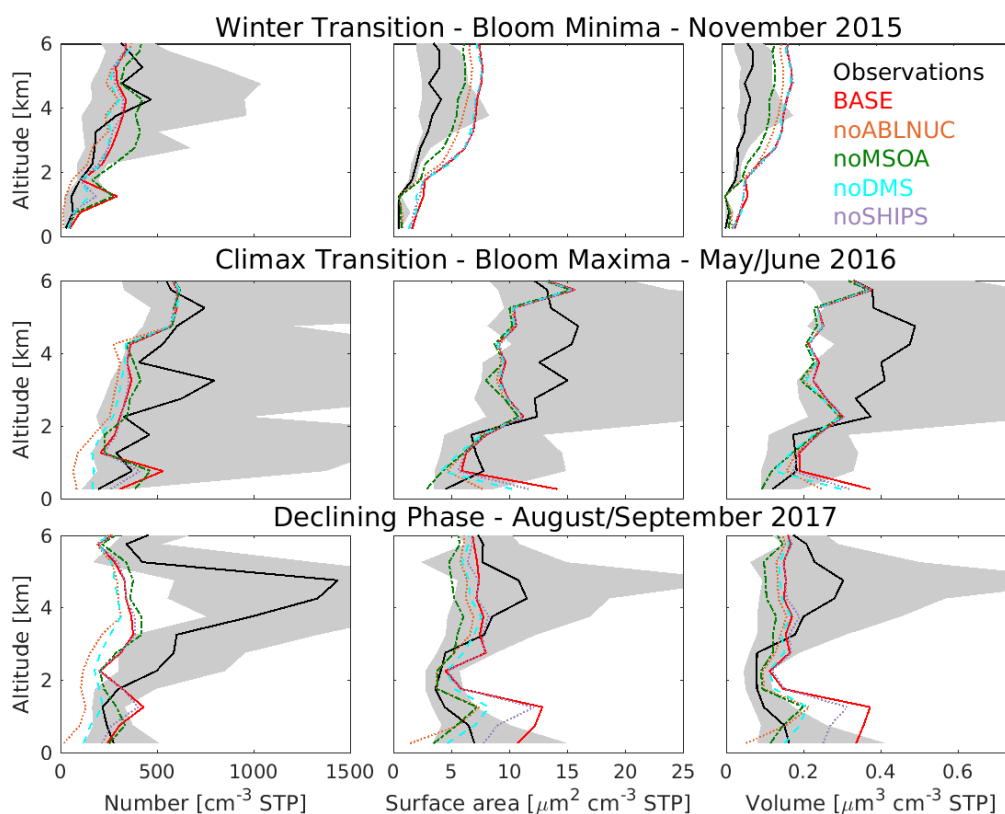
Figure 3: Vertical profiles of NAAMES campaign-median integrated SMPS observations at standard temperature and pressure (STP) for particles with diameters of 10 to 282 nm (black, with 25th-75th percentiles in grey) and for the five GEOS-Chem-TOMAS simulations described in Table 1 (color-coded as shown in legend). Linestyles: Solid: Observations, BASE; Dotted: noABLNUC, noSHIPS; Dash-dot: noMSOA; Dashed: noDMS.
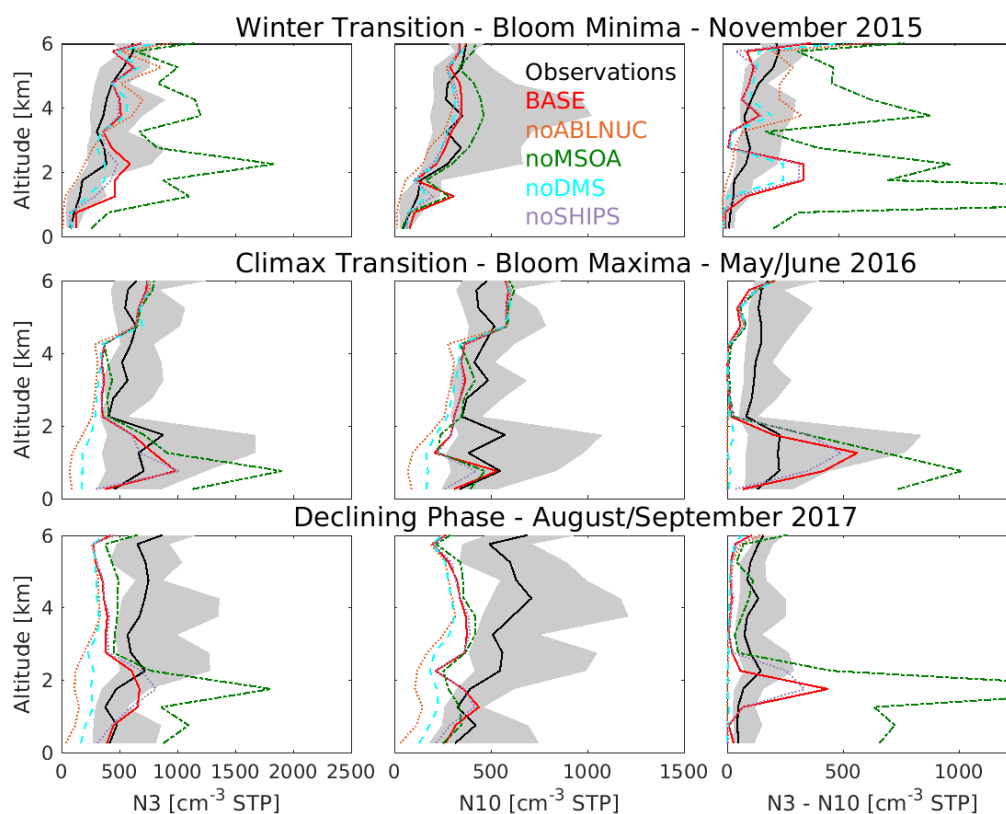
Figure 4: Vertical profiles of NAAMES campaign-median total number concentrations for particles with diameters larger than 3 nm (N3), 10 nm (N10) and between 3 to 10 nm (N3-N10) from CPC observations at standard temperature and pressure (STP) (black, with 25th-75th percentiles in grey) and for the five GEOS-Chem-TOMAS simulations described in Table 1 (color-coded as shown in legend). Linestyles: Solid: Observations, BASE; Dotted: noABLNUC, noSHIPS; Dash-dot: noMSOA; Dashed: noDMS.
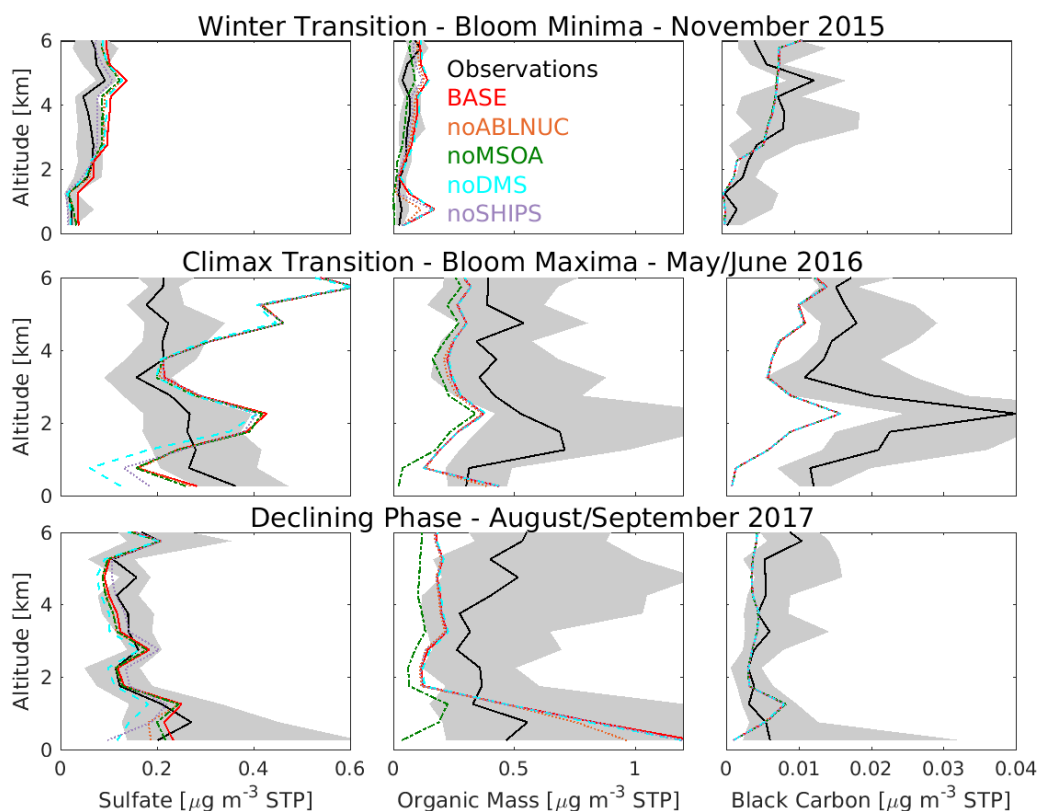
Figure 5: Vertical profiles of NAAMES campaign-median aerosol non-refractory sulfate and organic mass concentrations at standard temperature and pressure (STP) from Aerosol Mass Spectrometer and refractory black carbon from Single Particle Soot Photometer observations (black, with 25th-75th percentiles in grey) and for the five GEOS-Chem-TOMAS simulations described in Table 1 (color-coded as shown in legend). Simulated sulfate shown is non-sea-salt-sulfate. Linestyles: Solid: Observations, BASE; Dotted: noABLNUC, noSHIPS; Dash-dot: noMSOA; Dashed: noDMS.

1623
1624

1625
1626
Figure 6: Vertical profiles of NAAMES cruise-track campaign-median observed dimethyl sulfide

(DMS) mixing ratios (black, 25th-75th percentiles in grey) and for the five GEOS-Chem-TOMAS

simulations described in Table 1 (color-coded as shown in legend). Simulations BASE,

noABLNUC and noMSOA are nearly coincident. Linestyles: Solid: Observations, BASE; Dotted:

noABLNUC, noSHIPS; Dash-dot: noMSOA; Dashed: noDMS.
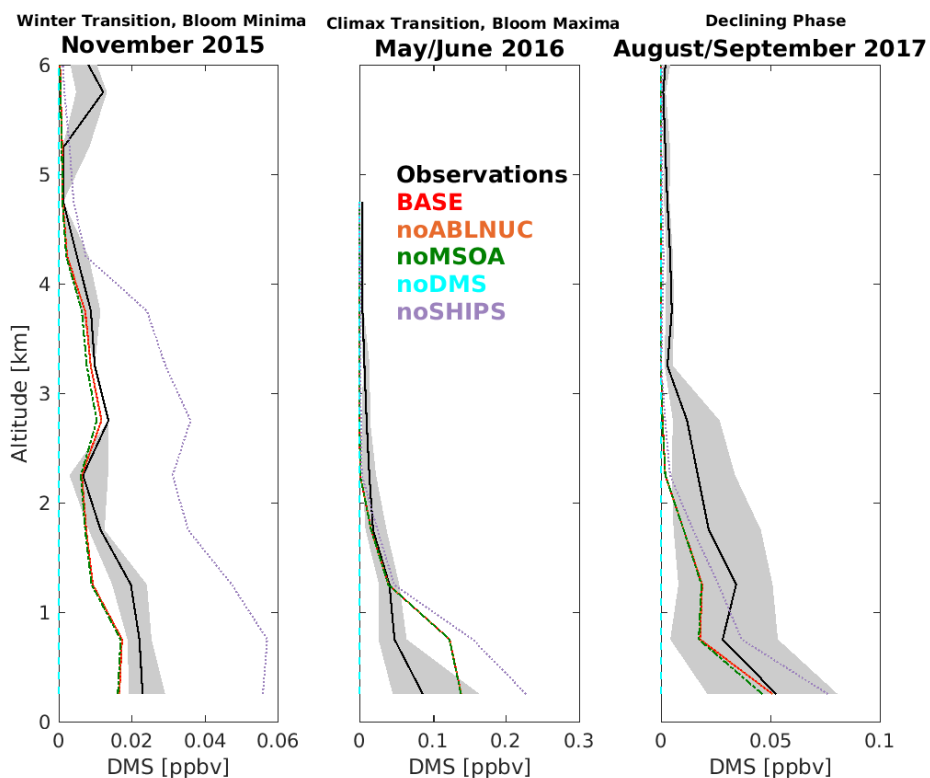
1632

1633
1634
1635
1636
1637
1638
1639
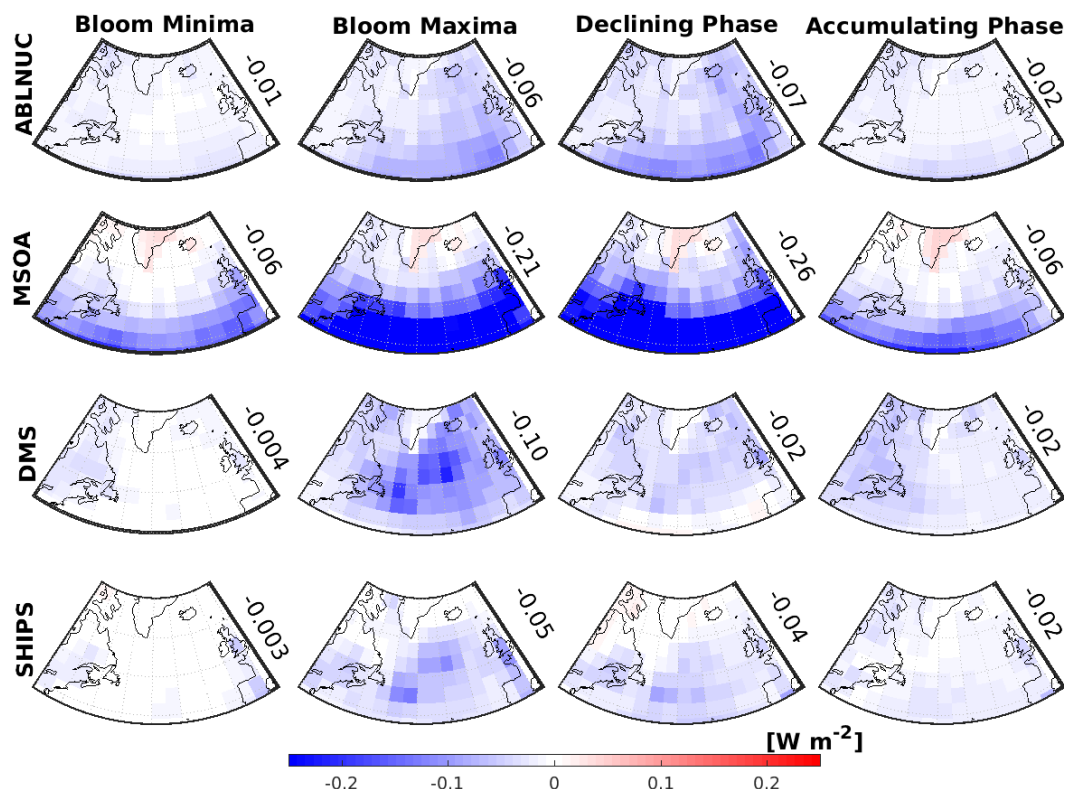
Figure 7: GEOS-Chem-TOMAS-simulated two-monthly-mean aerosol direct radiative effect (DRE) attributed to four key factors. Top row: Above boundary layer particle nucleation (ABLNUC); Second row: Particle growth by marine secondary organic aerosol (MSOA); Third row: Particle formation/growth due to DMS-oxidation products (DMS); Bottom row: Shipping emissions contribution to particles (SHIPS). DREs are in columns for the following time periods, October/November 2015 (Winter Transition, Bloom Minima), May/June 2016 (Climax Transition, Bloom Maxima), August/September 2017 (Declining Phase), and March/April 2018 (Accumulating Phase). DREs for ABLNUC, MSOA, DMS and SHIPS are calculated using the differences in the top-of-the-atmosphere solar flux between simulation BASE and respective sensitivity simulations (noABLNUC, noMSOA, noDMS, noSHIPS). Values shown are area-weighted-mean DREs over the region bounded by 40-60 ºN, 20-50 ºW.

1656

1657

1658

1659   Figure 8: GEOS-Chem-TOMAS-simulated two-monthly-mean aerosol cloud-albedo indirect

1660   radiative effect (AIE) attributed to four key factors. Top row: Above boundary layer particle

1661   nucleation (ABLNUC); Second row: Particle growth by marine secondary organic aerosol

1662   (MSOA); Third row: Particle formation/growth due to DMS-oxidation products (DMS); Bottom

1663   row: Shipping emissions contribution to particles (SHIPS). AIEs are in columns for the following

1664   time periods, October/November 2015 (Winter Transition, Bloom Minima), May/June 2016

1665   (Climax Transition, Bloom Maxima), August/September 2017 (Declining Phase), and

1666   March/April 2018 (Accumulating Phase). AIEs for ABLNUC, MSOA, DMS and SHIPS are

1667   calculated using the differences in the top-of-the-atmosphere solar flux between simulation BASE

1668   and respective sensitivity simulations (noABLNUC, noMSOA, noDMS, noSHIPS). Values shown

1669   are area-weighted-mean AIEs over the region bounded by 40-60 °N, 20-50 °W.

1670

1671

1672

Simulation	Description
BASE	Control simulation with GEOS-Chem-TOMAS model (GCT12.1.1) as described in Sect. 2.2
noABLNUC	Same as BASE, excluding the surrogate activation-type particle nucleation parameterization above the marine boundary layer to about 2 km altitude, as described in Sect. 2.2
noMSOA	Same as BASE, excluding the temperature-dependent marine organic vapors, forming marine secondary organic aerosol (MSOA)
noDMS	Same as BASE, excluding all emissions of DMS
noSHIPS	Same as BASE, excluding all ship emissions

1673

1674   **Table 1**: GEOS-Chem-TOMAS simulation acronyms. Simulations and methodology are

1675   described in detail in Sect. 2.2 and 2.3.

1676

1677

1678

Simulation	Nov 2015 Bloom Minima	May/June 2016 Bloom Maxima	Aug/Sept 2017 Declining Phase	Mar/Apr 2018 Accumulating	Annual Mean
BASE	0.17	0.40	0.12	0.31	0.23
noABLNUC	0.84	0.53	0.87	0.44	0.66
noMSOA	0.76	0.31	0.86	0.39	0.63
noDMS	0.43	0.20	0.43	0.11	0.29
noSHIPS	0.31	0.13	0.23	0.21	0.22

1679

1680

1681   **Table 2:** Mean fractional error (MFE) between observations and the five GEOS-Chem-TOMAS

1682   simulations described in Sect. 2.2 and Table 1 for the ship-track campaign-median aerosol size

1683   distributions shown in Fig. 2. A MFE of 0.50 or less indicates acceptable model-measurement

1684   agreement.